Near Threshold Electroproduction of J/Ψ at 11 GeV

May 4, 2012

the ATHENNA Collaboration [1]

(A new experiment proposal to JLab-PAC39)

J. Arrington, N. Baltzell, A. El Alaoui, D. F. Geesaman,
K. Hafidi (Co-spokesperson) [2], R. J. Holt, D. H. Potterveld,
P. E. Reimer
Argonne National Laboratory, Argonne, IL

X. Qian (Co-spokesperson) [3]
California Institute of Technology, Pasadena, CA

K. Aniol
California State University, Los Angeles, CA

J. C. Cornejo, W. Deconinck, V. Gray
College of William & Mary, Williamburg, VA

X. Z. Bai, H. X. He, S. Y. Hu, S. Y. Jian, X. M. Li,
C. Shan, H. H. Xia, J. Yuan, J. Zhou, S. Zhou
China Institute of Atomic Energy, Beijing, P. R. China

P. H. Chu, H. Gao, M. Huang, S. Jawalkar, G. Laskaris
, M. Meziane, C. Peng, Q. J. Ye, Y. Zhang, X. F. Yan
Duke University, Durham, NC

---

[1] **A** J/Ψ **TH**reshold **E**lectroproduction on the **N**ucleon and **N**uclei **A**nalysis
[2] kawtar@anl.gov
[3] xqian@caltech.edu

P. Markowitz
Florida International University, Miami, FL

A. Afanasev
The George Washington University, Washington, DC

F. J. Jiang, H. J. Lu, X. H. Yan
Huangshan University, Huangshan, P. R. China

K. Allada, A. Camsonne, J.-P. Chen, E. Chudakov,
J. Gomez, M. Jones, J. J. Lerose, B. Michaels,
S. Nanda, P. Solvignon, Y. Qiang
Jefferson Lab, Newport News, VA

M. Mihovilovič, S. Širca
Jožef Stefan Institute of University of Ljubljana, Slovenia

G. G. Petratos, A. T. Katramatou
Kent State University, Kent, OH

Y. Cao, B.T. Hu, W. Luo, M. Z. Sun,
Y.W. Zhang, Y. Zhang
Lanzhou University, Lanzhou, P. R. China

T. Holmstrom
Longwood University, Farmville, VA

J. Huang, X. Jiang
Los Alamos National Laboratory, Los Alamos, NM

J. Dunne, D. Dutta, A. Narayan, L. Ndukum,
M. Shabestari, A. Subedi, L. Ye
Mississippi State University, Mississippi State, MS

E. Cisbani, A. d. Dotto, S. Frullani, F. Garibaldi
*INFN-Roma and gruppo collegato Sanitá and Italian National Institute of
Health, Rome, Italy*

M. Capogni

INFN-Roma and gruppo collegato Sanitá and ENEA Casaccia, Rome, Italy

V. Bellini, A. Giusa, F. Mammoliti, G. Russo,
M. L. Sperduto, C. M. Sutera

INFN-Sezione di Catania, Catania, Italy

D. Y. Chen, X. R. Chen, J. He, R. Wang, H. R. Yang, P. M. Zhang

Institute of Modern Physics, Lanzhou, P. R. China

C. E. Hyde

Old Dominion University, Hampton, VA

L. El Fassi, R. Gilman

Rutgers University, Piscataway, NJ

S. Choi, H. Kang, H. Kang, Y. Oh

Seoul National University, Seoul, Korea

P. Souder and R. Holmes

Syracuse University, Syracuse, NY

W. Armstrong, H. Atac, A. Blomberg, D. Flay, E. Fuchey,
M. Paolone, N. Sparveris (Co-spokesperson) [4],
Z.-E. Meziani (Co-spokesperson/Contact) [5], M. Posik, E. Schulte

Temple University, Philadelphia, PA

K. Kumar, J. Mammei, S. Riordan

University of Massachusetts, Amherst, MA

T. Badman, S. K. Phillips, K. Slifer, R. Zielinski

University of New Hampshire, Durham, NH

---

[4]sparveri@jlab.org
[5]meziani@temple.edu

H. Badhdasaryan, G. D. Cates, M. Dalton, D. Day, D. Keller,
V. V. Nelyubin, K. Paschke, A. Tobias,
Z. W. Zhao (Co-spokesperson) [6], X. Zheng
University of Virginia, Charlottesville, VA

F. R. Wesselmann
Xavier University of Louisiana, New Orleans, LA

---

[6]zwzhao@jlab.org

Abstract

We propose to measure the electroproduction of J/Ψ meson cross section off a proton near threshold (4.05 GeV $<$ W $<$ 4.45 GeV and $|t - t_{min}|$ $<$ 2.5 GeV^2) with an 11 GeV electron beam. The high luminosity JLab 12 GeV upgrade electron beam combined with the large acceptance device SoLID in Hall A allow for a fully exclusive measurement of this process near threshold. The proposed measurement is sensitive to the non-perturbative gluonic interaction between the J/Ψ and nucleon and might reveal an enhancement of the cross section just above threshold. This in turn could be a manifestation of the important role of the conformal anomaly. A further consequence is whether or not J/Ψ-nuclear bound states would exist in nature. Such a measurement would open a new window to study QCD in the non-perturbative regime using charmonium as we contemplate a multi-phase program. Our total requested beam time for the first phase of measurements on proton is 60 days.

Contents

1 Physics Motivation

One of the fundamental goals of modern nuclear physics is to understand hadrons and nuclei starting with the basic ingredients of QCD namely quarks and gluons and their interactions. While significant progress has been made in exploring the theory in its perturbative regime much remains to be understood in the strong regime, particularly the part dominated by gluonic exchanges and interactions. Strong gluonic field configurations and interactions are responsible for most of the mass of nucleons and nuclei. Fundamental approaches such as lattice QCD, effective field theories or dual string theories (that would match QCD) could in principle shed light on confinement of hadrons and perhaps make predictions of novel phenomena of strong interactions.

In this proposal we aim to explore this strong interaction using a particular system that emphasizes the multiple gluonic exchange between two color neutral particles which do not share common valence quark, namely nucleons/nuclei and charmonia. It has long been argued that the force acting between nucleon/nucleus and J/Ψ is an attractive force, which has negligible mesonic ($D\bar{D}$) or multi-mesonic ($\rho\pi$) exchange contribution at low energies [1]. Since the nucleon/nucleus and J/Ψ are color neutral, this force is dubbed color Van der Waals force in analogy with the atomic-molecular physics case. This situation is unique in nuclear physics where a force exchanged between nucleons or hadrons is purely gluonic especially at low energy. A direct consequence of such an attractive force is the possible existence of a nuclear bound quarkonium state which was proposed more than 20 years ago by Brodsky, Schmidt and de Teramond [2] but has yet to be observed. A calculation using the operator product expansion (OPE) [3] to describe the low energy interaction of quarkonium with nuclei, in the limit where the mass of the charm quark is infinite, found that the J/Ψ binds in nuclear matter with about 10 MeV but the authors caution about possible large corrections due to confinement effects.

Due to the lack of experimental data, a timid but sustained theoretical activity on the subject followed over the past twenty years. For example, Kaidalov and Volkovitsky [4] argued that S-wave quarkonia can be found in nuclei with A $\geq$10 and with binding energy of few MeV, while de Teramond et al. [5] in an update to his original paper with Brodsky [2] estimated a binding energy of 2 MeV in ^{12}C and 10 MeV in ^{208}Pb, while Shevchenko [6] pointed in a later work that the interaction of charmonium-nucleon is so small that the potential depth for nuclear bound state may only for nuclei with A > 200. Applying QCD sum rules Hayashigaki [7] finds a 4 to 7 MeV binding of the J/Ψ in nuclear matter. Yokokawa, Sasaki, Hatsuda and Hayashigaki [8] performed a first lattice study in the quenched approximation of low energy charmonium-hadron interaction to determine the scattering length. But more recently Kawanai and Sasaki [9] calculated the charmonium-nucleon potential from the equal-time Bethe-Salpeter amplitude through the effective Schrödinger equation and found that the charmonium-nucleon potential is weakly attractive at short distances and exponentially screened at large distances. Finally, Tsushima, Lu, Krein and Thomas [10, 11] have recently explored the J/Ψ-nuclear bound states and found that the attractive potential that originate from the D and D^* meson

loops in the J/Ψ in nuclear medium should produce bound states.

Many of the J/Ψ photoproduction experiments have been performed at high photon energies and low t or in the case of electroproduction at large center of mass energy s and low t (see Refs. [12, 13, 14, 15, 16, 17, 18, 19]) usually considered as a diffractive production. Experiments in the threshold region are few and were performed soon after the discovery of the J/Ψ particle more than 35 years ago [20, 21, 22, 23]. In particular, the measurements of Cornell [21] and SLAC [23] show large discrepancies at photon energy around 10 GeV.

It is fair to say that not much is known in the region where the energy of the photon is just above 8.2 GeV and where t is about 2 GeV, namely the threshold region. With Jefferson Lab at 12 GeV, we enter a new kinematic domain where the electro/photo-production of charmed hadrons at threshold becomes possible. It is precisely a region well suited for the investigation of the QCD Van der Waals interaction, since as we approach the threshold and due to the conformal scale anomaly of the low energy J/Ψ-nucleon interaction [24, 25] the non-perturbative part of the interaction vanishes more slowly then the perturbative part. In his paper of 1998 [25], Kharzeev considered explicitly the possible enhancement of the threshold cross section due to this conformal scale anomaly which correspond to a diagram where the coupling of the quarkonium to the nucleon occurs through a triangle gluonic lines (see Fig. 1). As shown in Fig. 2, the scattering amplitude in the threshold region is also dominated by its real part in contrast to the case of high energy.

Later Brodsky, Chudakov, Hoyer and Laget [26] discussed the photoproduction of charm near threshold and invoked the two-gluon exchange mechanism in the production. These authors also considered the possible enhancement of the cross section at threshold due to a strong interaction beyond two-gluon exchanges as shown in Fig. 3. Whereas Sibirtsev, Krewald and Thomas [27] attributed the mechanism of the J/Ψ photoproduction at low energies and large t to a mechanism different from pomeron or two-gluon exchange. They considered the possibility of the exchange of an axial vector trajectory that couples with the axial form factor of the nucleon in this case also enhancing the cross section at threshold.
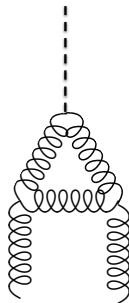
Figure 1: Anomaly diagram which dominate the cross section interaction at threshold.
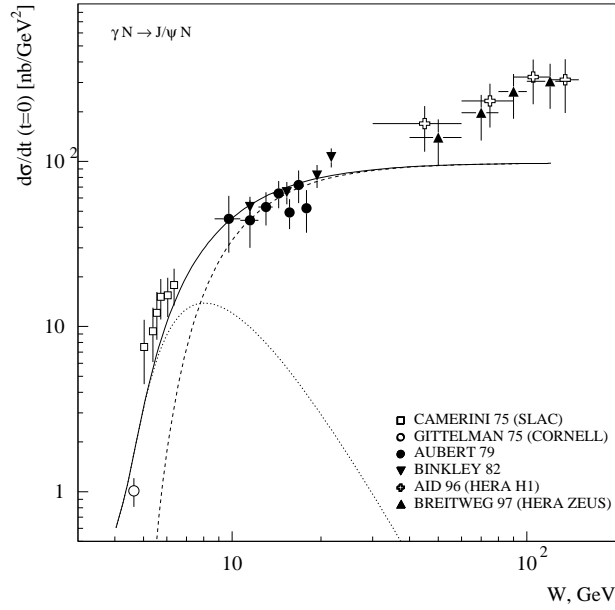
Figure 2: Forward J/Ψ photoproduction data compared to the results of [25] with (solid line) and without (dashed line) the real part of the amplitude.

.
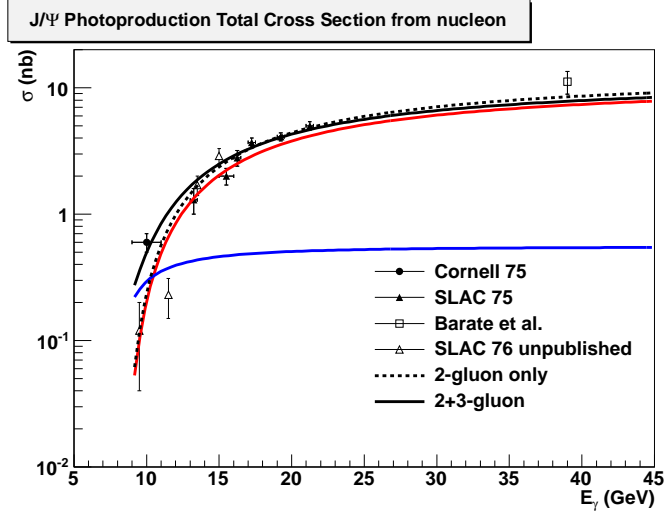
Figure 3: The 2-gluon model is shown as dotted black line. The (2+3)-gluon model is shown as solid black line. Furthermore, the 2-gluon contribution and 3-gluon contribution in the (2+3)-gluon model are shown as red and blue lines as well. Data are from "Cornell 75" [21], "SLAC 75" [20], "SLAC 76" [23] and "Barate et al." [15].

9

At first, the charmonium production near the threshold region would not seem to lend itself to calculations using pQCD similar to the case of deep inelastic scattering at large Q^2. However, a closer look reveals a new scale at play, namely the mass of heavy quarks, which when compared to Λ_{QCD} enables a perturbative approach to evaluate the scattering amplitude of the process. This fact was used a while ago to derive charm photoproduction sum rules in a way similar to deep inelastic scattering [28, 29, 30].

In the reaction $\gamma^* + N \rightarrow J/\Psi + N$, the production mechanism at threshold can be viewed in a way similar to the J/Ψ elastic scattering off a nucleon at small relative velocity. The coupling of the soft gluonic fields to the nucleon, at low Q^2 is determined by the low-energy theorem in QCD based on the anomaly in the trace of the energy-momentum tensor. The J/Ψ-nucleon scattering amplitude is proportional to the nucleon matrix element of the following gluon operator [31]:

$$\langle N|\frac{1}{2}\vec{E}^a \cdot \vec{E}^a|N\rangle = \frac{4\pi^2}{b}\langle N|\theta^\mu_\mu|N\rangle + 2\pi\alpha_s\langle N|\theta^{00}_G|N\rangle, \tag{1}$$

where $\vec{E}^a$ represents the chromo-electric field, $\theta^{\mu\nu}_G$ is the energy-momentum tensor of the gluon field, θ^μ_μ is the anomalous trace of the full energy-momentum tensor in QCD in the chiral limit, b is the coefficient in the QCD beta function with three light (massless in the chiral limit) quarks and α_s is the QCD coupling.

It is argued [31] that this matrix element is bound by

$$\langle N|\frac{1}{2}\vec{E}^a \cdot \vec{E}^a|N\rangle \geq \frac{4\pi^2}{b}2m^2_N \tag{2}$$

In a measurement of electroproduction close to the threshold region, and unlike at high energy, the real part of the scattering amplitude contribution dominates compared to the imaginary part even though the allowed exchanges are purely gluonic. This contribution probes the matrix element represented by $\langle N|\theta^\mu_\mu|N\rangle = 2m^2_N$. Hence, in a threshold measurement we probe the conformal anomaly contribution to the low energy $J/\Psi - N$ interaction comparable to a Higgs-like coupling [7]. Furthermore, the determination of an upper limit of the strength of this interaction will help determine whether or not a nucleon-J/Ψ bound state due to the Van der Waals color forces would exist.

The high luminosity and large solid angle offered by the Jefferson Lab 12 GeV energy upgrade combined with the SoLID detector in Hall A is a unique tool to start an investigation program of the J/Ψ-nucleon interaction. Hence, we propose, in a first phase, the measurement of the cross section of electroproduction of J/Ψ on a nucleon at threshold. These measurements at threshold have not been revisited since the 70s. The precision and energy range close to threshold of the proposed measurement will best probe the possible enhancement of the cross section due to the contribution of the conformal anomaly in the threshold region. Threshold enhancements due to on-shell

---

[7]The coupling of the contact term is sensitive to the entire mass of nucleon, and as such is similar to the Higgs coupling.

rescattering or quasi-bound states around threshold have been observed in several observables such as $e^+e^- \rightarrow p\bar{p}, \Lambda\bar{\Lambda}, \Sigma^0\bar{\Sigma}_0, \Lambda\bar{\Sigma}_0$ [32] as well as in the J/Ψ radiative decays, e.g. $J/\Psi \rightarrow p\bar{p}\gamma$ [33]. The proposed experiment aims at observing such enhancement in the J/Ψ-proton system and offers the capability to explore the region below threshold if there are hints of an enhancement of the cross section just above threshold. Furthermore, the proposed cross section measurement could also shed light on the existance of predicted super-heavy N^* with hidden charm with a mass around 4.3 GeV [34].

In a second phase we shall explore the interference of the Bethe-Heitler amplitude with that of the J/Ψ electroproduction to attempt a determination of the relative contribution of the real to the imaginary part of the scattering amplitude. Moreover, a study of the angular distribution of the J/Ψ decay can reveal whether the J/Ψ was originally produced from an octet or singlet state.

Finally, studies of J/ψ production and propagation in the nuclear medium is the natural extension of the proposed measurements on a nucleon. The study of multi-gluon QCD Van der Waals forces in nuclei is believed to shed new light on their possible role in J/ψ-nuclear bound states [2, 3, 4, 5, 2, 6, 7, 8, 9]. Another related challenge is the in-medium properties of charmonia as well as the possible restoration of the chiral symmetry in the nuclear medium, which is closely connected to the modifications of masses and widths of mesons when embedded in the nuclear environment [10]. For these studies, it is important to find the appropriate kinematical conditions to produce J/ψ at rest, or with small momentum relative to the nucleus. Therefore, measurements at threshold and even sub-threshold look promising [35].

2   Experimental Status

At JLab Hall C, a photoproduction experiment (E03-008) was performed in the *subthreshold* regime using the CEBAF at 6 GeV. Unfortunately no signal was observed after one week of beam scattering of a ^{12}C target [35]. This experiment allowed to set a limit on the cross section, which was found to be consistent with the quasi-free production. The experiment used a bremsstrahlung beam produced in a copper radiator by the 6 GeV incident electron beam . The pair of spectrometers (HMS and SOS) of Hall C were used to detect the pair of leptons resulting from the decay of the J/Ψ. More recently, a proposal [36] for the 12 GeV upgrade of Hall C was considered by the PAC32 and conditionally approved. The authors proposed the use of bremsstrahlung photon beam created in a radiator to look at the photoproduction at threshold in a series of nuclei. The physics goal was to measure the photoproduction cross section on hydrogen and then investigate the A dependence of the propagation of the J/Ψ in the nuclear medium. In this proposal, only the J/Ψ is detected through the detection of the decay leptonic pair.

For the proposed measurements, we argue that electroproduction rather than photoproduction is the preferred way to perform this experiment at threshold for reasons listed below:

- The virtual photon energy and momentum are well defined by detecting the scattered electron in this rapidly varying kinematic region.

- In contrast to the photon measurements, the radiation background created in the Hall is significantly reduced allowing for the experiment to run for a good period of time without the limitation due to the radiation budget of the Hall.

- The achievable virtual photon flux using CEBAF 12 GeV with a luminosity up to 10^{37} N cm^{-2} s^{-1} is critical in this region of rapidly falling cross sections.

- Full exclusivity is required by detecting the scattered electron, the J/Ψ decay leptonic pair and with/without proton to clean up any background contamination in this low cross section production process on hydrogen.

3   The Proposed Experiment

3.1   Overview

We propose to measure the J/Ψ electroproduction cross section near production threshold by using the Solenoidal Large Intensity Device (SoLID), one of the major new equipments in the Hall A 12 GeV era. Two groups of experiments using SoLID, parity violation deep inelastic scattering (SoLID-PVDIS) [37] and semi-inclusive deep inelastic scattering (SoLID-SIDIS) [38, 39, 40], have been approved with A rating. Our proposed measurement of J/Ψ electroproduction requires coincident detection of electrons, positrons as well as protons. Therefore the configuration of SoLID will be similar to that of SoLID-SIDIS. In addition, the standard Hall A 15 cm liquid Hydrogen target will be located upstream at z = -10 cm relative to the target center of the SoLID-SIDIS setup.

The layout of the experiment is shown in Fig. 4. The detector system consists of forward and large angle detectors. With a polar angle coverage from 8° to 15°, the forward angle detectors can identify charge particles with momenta ranging from 0.8 GeV to 7.0 GeV. Particle tracking in the forward angle region is provided by 5 layers of GEM detectors. The particle identification will be obtained from a combination of an electromagnetic calorimeter (EC), a gas Cerenkov counter (GC), and a layer of Multi-gap Resistive Plate Chamber (MRPC). The polar angle coverage for the large angle detectors is from 15° to 25°. The large angle detectors can detect electrons and positrons with momentum above 2.5 GeV. The particle identification will be achieved by an electromagnetic calorimeter.

The reaction of interest is $e + p \rightarrow e' + J/\Psi(e^-, e^+) + p$ where J/Ψ is detected through its decay in a lepton pair (e^+, e^-) with 5.94% branching ratio. Primary detection channels include a 4-fold coincidence, which consists of detecting the scattered electron, the recoil proton, and the leptonic pair $(e^+ e^-)$ from J/Ψ decay, and a 3-fold coincidence, similar to the 4-fold coincidence but without proton detection. In the 3-fold coincidence channel, the full kinematics of the recoil proton can be reconstructed through energy and momentum conservation. Since the recoil proton is not detected, the total number of events and the kinematical coverage are greatly enhanced compared to the 4-fold coincidence channel. Possible background in the 3-fold coincidence channel can be investigated fully with the 4-fold coincidence channel which offers a better signal to noise ratio. Fig. 4 illustrates the particle detection scheme of the 4-fold coincidence. The scattered electron and the recoil proton will be detected by the forward angle detector, while the electron-positron pair from J/Ψ decay will be mostly detected by the large angle detector.

3.2   Kinematic

For the exclusive electroproduction of J/Ψ on a proton, the main kinematic variables are: Q^2 (the four-momentum transfer of the electron), W (the center of mass energy of the
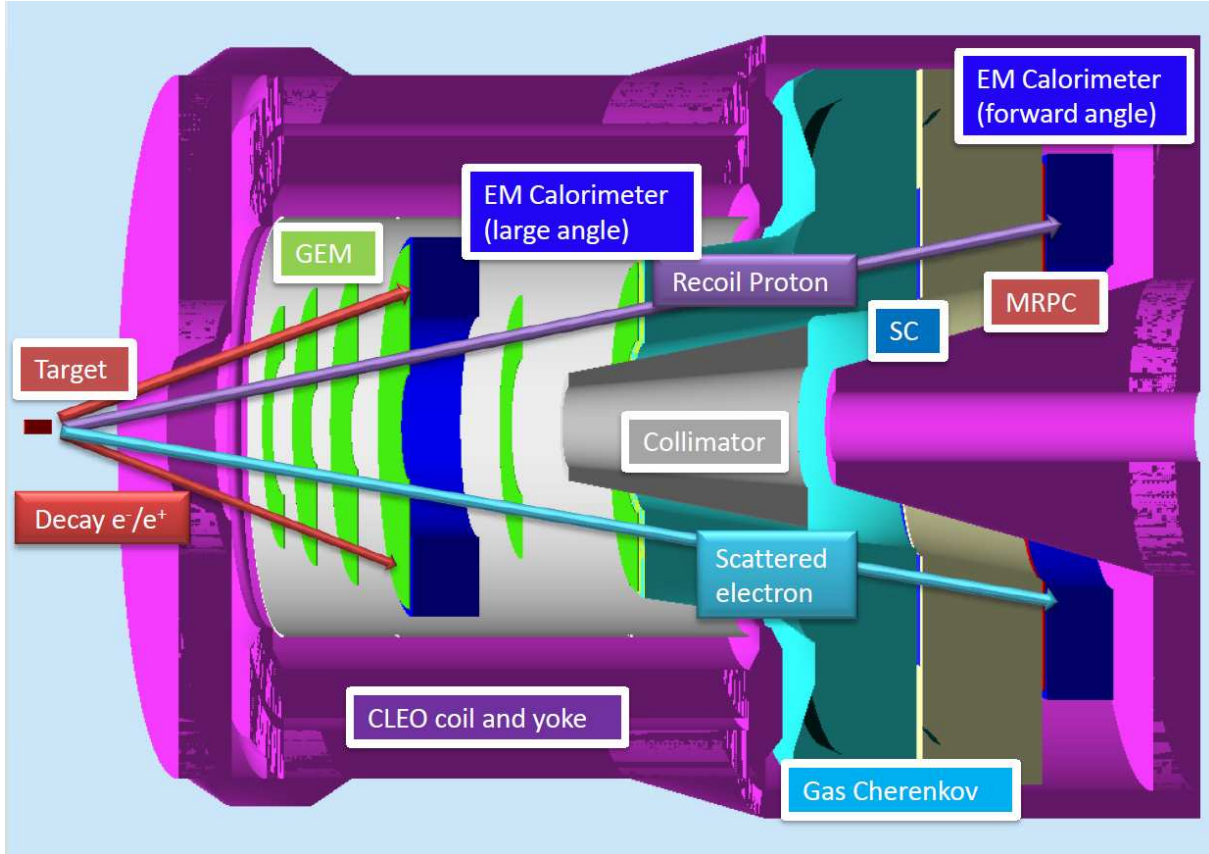
Figure 4: The experimental layout of the SoLID for the proposed experiment. The sub-detectors are labeled and the four final state particles are displayed by arrows. The scattered electron and recoil proton are detected by the forward angle detector. There are five layers of GEM detectors inside the coils upstream of the gas Cherenkov. The forward angle EM calorimeter provides the trigger and an additional electron/pion separation. The Multi-gap Resistance Plate Chamber (MRPC) provides coincidence timing. The electron-positron pair from J/Ψ decay primarily detected by the large angle detector. Four layers of GEM detectors are placed inside the coils. Three of them are common GEMs shared with the forward angle detector. The large angle EM calorimeter provides the trigger, the coincidence timing and the electron/pion separation. The 15 cm long liquid hydrogen target is located at z = -10 cm relative to the target center in SoLID-SIDIS experiments.
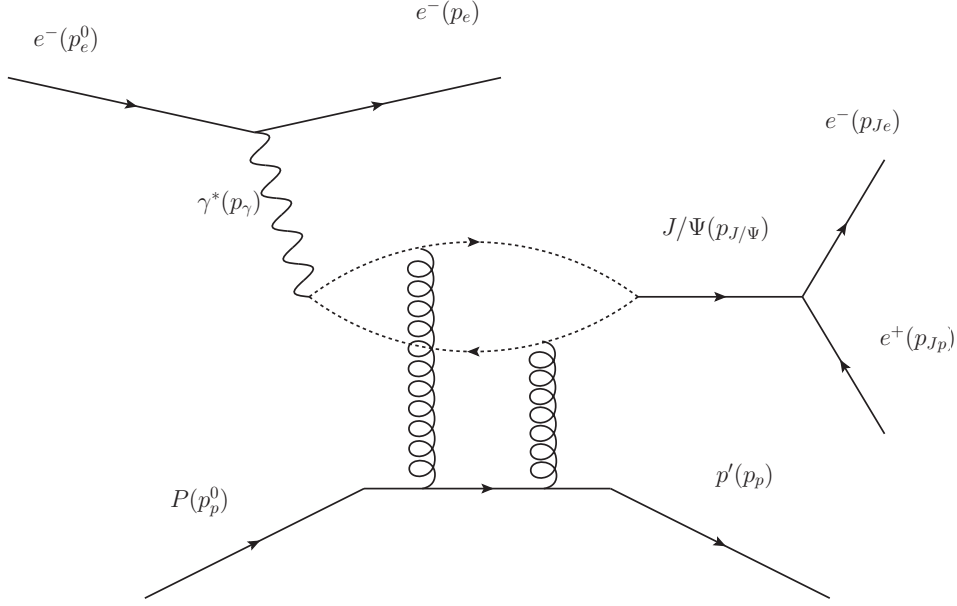
Figure 5: The kinematics of the exclusive electroproduction of J/Ψ on a proton assuming a 2-gluon exchange interaction. The four-momentum of all particles are defined. The relevant kinematic variables including Q^2, t and W are defined in the text.

.

virtual photon and proton system), t (the four-momentum transfer of the proton [8]).

$$
\begin{aligned}
Q^2 &= -(p_e^0 - p_e)^2 \\
W &= \sqrt{2\nu \cdot M_p + M_p^2 - Q^2} \\
t &= (p_p^0 - p_p)^2 = (p_\gamma - p_{J/\Psi})^2.
\end{aligned}
\tag{3}
$$

Here, p_e^0, p_e, p_p^0, p_p, p_γ, $p_{J/\Psi}$, p_{Je} and p_{Jp} are the four-momentum of the initial electron, the scattered electron, the initial proton, the recoil proton, the virtual photon , the J/Ψ, the J/Ψ decay electron and positron, respectively. M_p is the mass of proton. Fig. 5 shows the kinematics.

Furthermore, due to the kinematic limitation, the t coverage is defined with its maximum and minimum values:

$$
t_{min} = \left[\frac{m_{\gamma^*}^2 - m_p^2 - m_{J/\Psi}^2 + m_p^2}{2W} \right]^2 - (p_{\text{init}}^{cm} - p_{\text{final}}^{cm})^2
$$

$$
t_{max} = \left[\frac{m_{\gamma^*}^2 - m_p^2 - m_{J/\Psi}^2 + m_p^2}{2W} \right]^2 - (p_{\text{init}}^{cm} + p_{\text{final}}^{cm})^2.
\tag{4}
$$

$$
\tag{5}
$$

[8]also for the four-momentum transfer between the virtual photon and the J/Ψ.
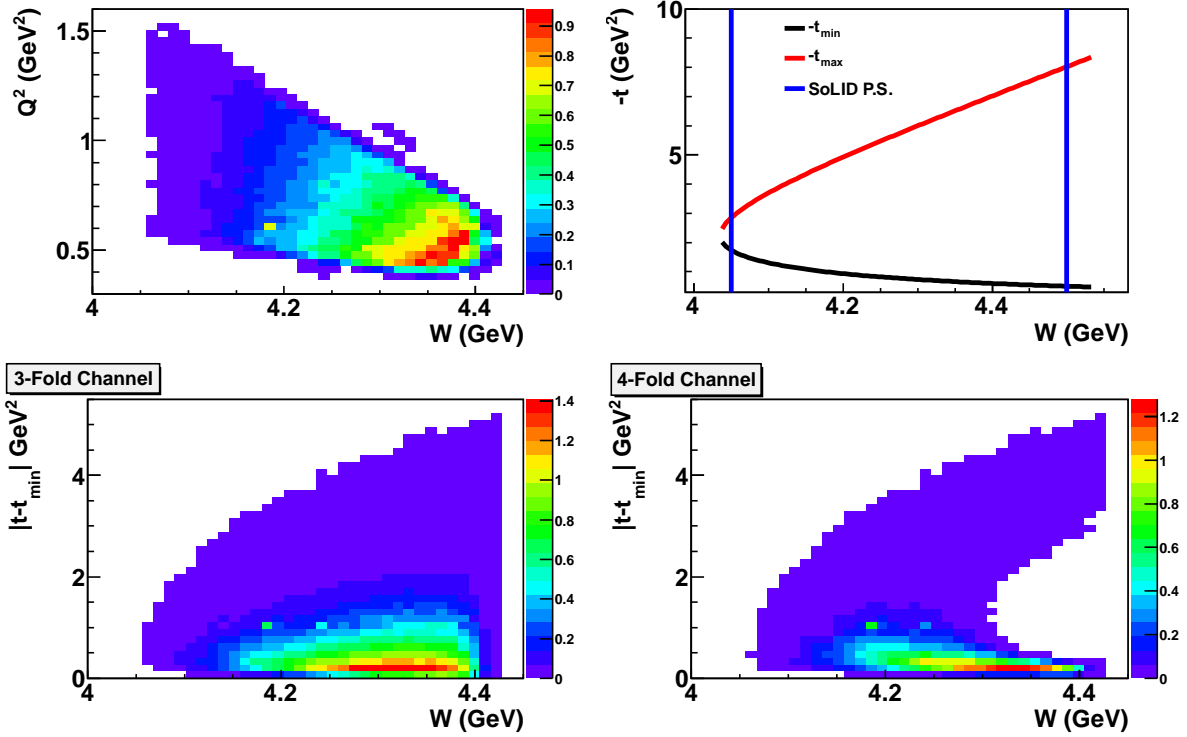
Figure 6: The coverage of Q^2 vs. W (top left), t vs. W (top right), $|t - t_{min}|$ vs. W for 3-fold coincidence channel, (bottom left) and for 4-fold coincidence channel (bottom right) are shown. Since the detection of recoil proton is required, the $|t - t_{min}|$ coverage for the 4-fold coincidence channel is reduced.

The top right panel of Fig. 6 shows the kinematic coverage of W and associated t_{min} and t_{max}. With the large acceptance of the SoLID detector, we can cover a wide range of W near threshold ($W_{threshold} \sim 4.035~GeV$). The expected Q^2 vs. W coverage and $|t - t_{min}|$ vs. W are also presented for both 3-fold and 4-fold coincidence channels in Fig. 6.

3.3 Summary of changes to the SIDIS setup

The SoLID design (more details can be found in Sec. 6) for this proposal is very similar to the proposed setup for the SIDIS measurement. Nevertheless we require a few changes in order to optimize the setup for the desired measurements:

- Enlarge the opening angle of the front yoke to 26 degrees.

- The large angle calorimeter and the fourth layer of GEM tracker will be moved toward the target by about 12 cm.

- The outer radius of first three layers of GEM chambers need to enlarged by 10 cm in order to match the acceptance of the large angle calorimeter.

- The target center will be moved to -10 cm upstream relative to the target center of SoLID-SIDIS setup.

Here, the shift of the target position is needed to optimize the forward angle detection for the scattered electron and proton. The move of the detector system is to optimize the large angle detection of the electron-positron pair from the J/Ψ decay. The standard Hall A 15 cm long LH_2 target (see Sec. 6.6) will be used.

3.4   Rates

3.4.1   Physics Rate

The cross section of J/Ψ electroproduction is calculated using equivalent photon approximation [41]:

$$\frac{d^5\sigma}{d\Omega_e dP_e d\Omega_p} = \Gamma \frac{J}{2\pi} \cdot \frac{d\sigma}{dt}. \tag{6}$$

Here, Ω_e, Ω_p are the solid angles of the scattered electron and recoil proton, respectively. And P_e is the momentum of the scattered electron. Γ is the equivalent photon flux defined as

$$\Gamma = \frac{\alpha_{EM}}{2\pi^2} \frac{P_e}{P_e^0} \frac{K_{eq}}{Q^2} \frac{1}{1-\epsilon}, \tag{7}$$

where P_e^0 is the initial electron momentum, and α_{EM} is the fine coupling constant. Furthermore, $K_{eq} = (W^2 - M_p^2)/(2M_p)$ and ϵ

$$\epsilon = \frac{1}{1 + \frac{2|q^2|}{Q^2} \tan^2 \frac{\theta_e}{2}}, \tag{8}$$

is the polarization of virtual photon. Here, q is the three-momentum of the virtual photon, and θ_e is the polar angle of the scattered electron. In addition, the $J/(2\pi)$ in Eqn. 6 is the Jacobian

$$\frac{dt}{d\Omega_p} = \frac{J}{2\pi}. \tag{9}$$

The differential cross section $\frac{d\sigma}{dt}$ of Eqn. 6 is calculated assuming 2-gluon exchange only or a hybrid of 2-gluon and 3-gluon exchange [42] [9] at fixed W:

$$\frac{d\sigma_{2g}}{dt} \sim N_{2g}(1-x)^2 e^{1.13t},$$

$$\frac{d\sigma_{3g}}{dt} \sim N_{3g}(1-x)^0 e^{1.13t}, \tag{10}$$

---

[9]We also refer the hybrid model as (2+3)-gluon exchange.
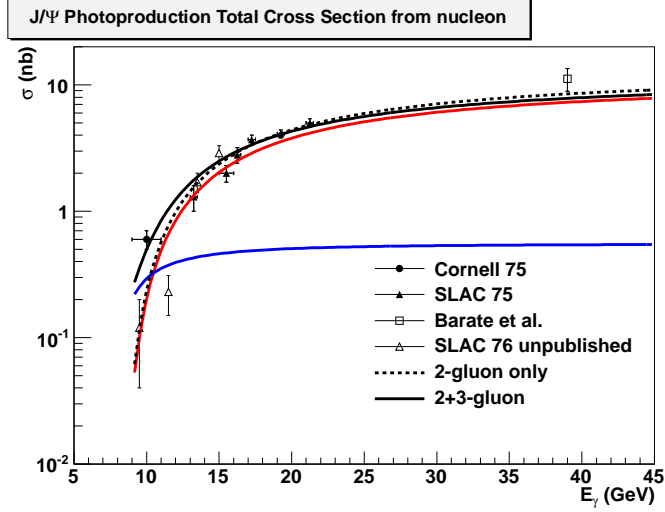
Figure 7: The 2-gluon only model is shown as dotted black line. The (2+3)-gluon model is shown as solid black line. Furthermore, the 2-gluon contribution and 3-gluon contribution in the (2+3)-gluon model are shown as red and blue line as well. Data are from "Cornell 75" [21], "SLAC 75" [20], "SLAC 76 unpublished" [23] and "Barate et al." [15].

where

$$x = \frac{2M_p M_{J/\Psi} + M_{J/\Psi}^2}{s - M_p^2}. \tag{11}$$

where $s = W^2$. Eqn. 11 shows that near threshold, the 2-gluon interaction is more suppressed than the 3-gluon due to the presence of $(1 - x)^2$. The total cross section of the J/Ψ production is then obtained by

$$\sigma_{tot} = \int_{t=t_{min}}^{t=t_{max}} \frac{d\sigma}{dt} dt. \tag{12}$$

Near threshold, as shown in the top right panel of Fig. 6, the total cross section will be smaller since the phase space coverage of t is reduced. The fit of the 2-gluon model and (2+3)-gluon model [42] are shown in Fig. 7. In this fit, the unpublished data from SLAC76 [23] are not included. Clearly, if the 3-gluon exchange is present near threshold, it would lead to an enhancement of the cross section.

The J/Ψ decay angular distribution [43] is assumed to be:

$$W(\cos\theta) = \frac{3}{8\pi}(1 - r + (3r - 1)\cos^2\theta), \tag{13}$$

where

$$r = \frac{\epsilon R}{1 + \epsilon R}, \tag{14}$$

18
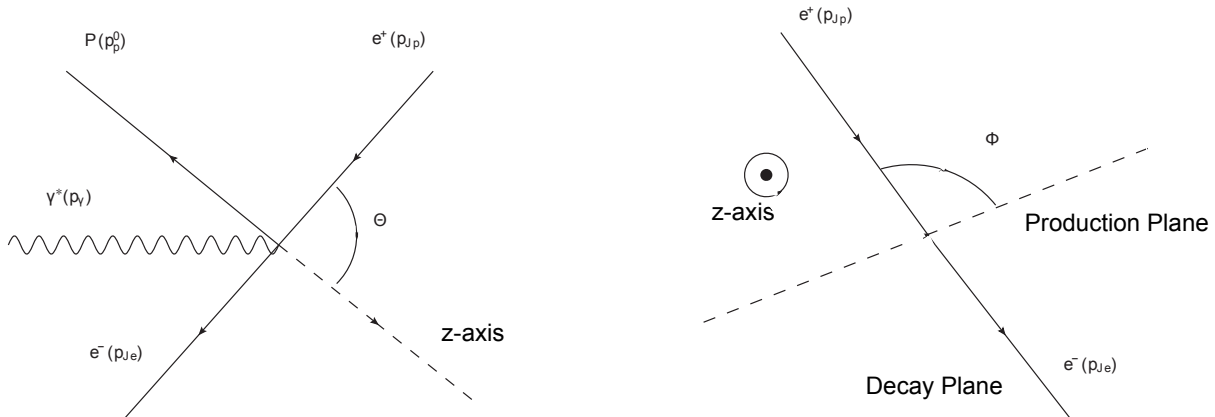
Figure 8: The θ (polar) and ϕ (azimuthal) angles describing the decay angular distribution of J/Ψ in its rest frame. The production plane is defined by the momentum vectors of the virtual photon and the recoil proton. The decay plane is defined by the momentum vectors of the decay electrons and positrons.

	2-gluon only	(2+3)-gluon
4 fold	0.7k	2.9k
3 fold	2.1k	8.1k

Table 1: Total number of events at 10^{37} N cm^{-2} s^{-1} luminosity and 50 days of running.

and

$$R = \left(\frac{aM_{J/\Psi}^2 - Q^2}{aM_{J/\Psi}^2} \right)^n - 1, \tag{15}$$

with $a = 2.164$ and $n = 2.131$ [44]. Here, θ is the polar angle of the positron in the J/Ψ rest frame (see Fig. 8). The z-axis is defined using the momentum direction of the recoil proton in the J/Ψ rest frame. More details about the decay kinematics can be found in Ref. [45].

Models of cross section and decay angular distribution are then combined with the acceptance calculated from GEANT Monte Carlo to estimate the rate. The 15 cm long target results in an average 10% reduction in acceptance compared with a point-like target. We request a luminosity of 10^{37} N cm^{-2} s^{-1} and 50 PAC days. The overall detection efficiency is assumed to be 85%. The accumulated total number of expected events are summarized in Table. 1 for both 3-fold and 4-fold coincidence channels.

3.4.2 Single Rates

Single event rates are listed in Table. 2. We have assumed a 3 μA beam current, a 15 cm long liquid hydrogen target. The overall luminosity is about 10^{37} N cm^{-2} s^{-1}. High-

energy photon (relevant to the electron trigger at both forward and large angle detector) rates are estimated using the π^0 rates, where the π^0 production cross section is assumed to be twice the sum of π^+ and π^- at high energy. We compared the rate estimations from Whitlow [46]/QFS [47] and Wiser [48] with data from E06-010 for HRS and a GEANT based model for the BigBite spectrometer. Corrections were applied to match the data. Details can be found in Ref. [49]. The single electron rate includes contribution of the DIS from the Whitlow fits as well as the contribution of "photon-induced" electrons, including electrons from π^0 decay, and electrons generated by photons when they pass through materials. The low energy cut-off for the forward detection is about 0.7 GeV. The low energy cut-off for the large angle detection is 2.5 GeV from the trigger threshold. In the single rate estimation, the 85% detection efficiency was not applied.

Process	Rate Forward angle 11 GeV	Rate Large angle 11 GeV
single e^-	340 kHz	35.0 kHz
high energy photon	7.5 MHz	0.4 MHz
single π^+	11.0 MHz	0.25 MHz
single π^-	7 MHz	0.18 MHz
single proton	3.3 MHz	0.19 MHz

Table 2: Single rates for charged particles and high-energy photons detected at forward and large angles with an 11 GeV beam. The high energy photon cut-off is 0.7 (2.5) GeV at forward (large) angle.

3.5 Trigger Setup and DAQ

The default trigger will be a triple coincidence trigger combining the electron and positron from the J/Ψ decay (high-energy electron triggers by the large angle detector and also part of the forward angle detector), and the scattered electron (the low-energy trigger by the forward angle detector). In practice, with 30 sectors, singles' trigger will be first generated in each sector and then coincidence trigger will be formed between sectors.

3.5.1 High-energy Single Electron Trigger

In the large angle side, the trigger is provided solely by the large angle calorimeter with high threshold (2.5 GeV). With the online hadron rejection $R_{LC} = 20$ [38] from the calorimeter, the electron rate at large angle T_L^e is expected to be

$$T_L^e(11 \text{ GeV}) \quad = \quad Y_L^e + Y_L^\gamma + \frac{Y_L^h}{R_{LC}}$$

$$= \quad 35 + 396 + \frac{450}{20} = 450 \text{ kHz} \tag{16}$$

Since tracking is necessary to differentiate the positive charged particle from the negative one, the online rate of the high-energy positron trigger is the same as the high-energy electron trigger.

   In the forward angle side, the high-energy electron trigger is provided by a coincidence of the calorimeter and the gas Cherenkov. With the online hadron rejection $R_{FC} = 10$ from the calorimeter, and the online photon rejection $R_{GC} = 20$ from the gas Cherenkov, the rates are expected to be:

$$\begin{aligned} T_F^e(11 \text{ GeV}) &= Y_F^e + \frac{Y_F^\gamma}{R_{GC}} + \frac{Y_F^h}{R_{FC} \cdot R_{GC}} \\ &= 170 + \frac{120}{20} + \frac{190}{20 \cdot 10} = 177 \text{ kHz}. \end{aligned} \tag{17}$$

Therefore, the total rate of the high-energy trigger is about 627 kHz.

3.5.2 Low-energy Single Electron Trigger

In the forward angle, the low-energy electron trigger is provided by a coincidence of the calorimeter and the gas Cherenkov counter. With the online hadron rejection $R_{FC} = 10$ from the calorimeter, and the online photon rejection $R_{GC} = 20$ from the gas Cherenkov, the rate is expected to be:

$$\begin{aligned} T_F^e(11 \text{ GeV}) &= Y_F^e + \frac{Y_F^\gamma}{R_{GC}} + \frac{Y_F^h}{R_{FC} \cdot R_{GC}} \\ &= 340 + \frac{7500}{20} + \frac{21000}{20 \cdot 10} = 820 \text{ kHz} \end{aligned} \tag{18}$$

3.5.3 Coincidence Rates

The triple coincidence rate is then estimated as

$$\begin{aligned} R_{trigger} &= T_F^e \cdot 50 \text{ } ns \cdot (T_F^e + T_L^e) \cdot 50 \text{ } ns \cdot (T_F^e + T_L^e) \\ &= 820 \times 10^3 \cdot 50 \times 10^{-9} \cdot 627 \times 10^3 \cdot 50 \times 10^{-9} \cdot 627 \times 10^3 \\ &\sim 800 Hz. \end{aligned} \tag{19}$$

Here, we have assumed a 50 ns triple coincidence windows. Therefore, the final coincidence rate for this experiment at 10^{37} N cm^{-2} s^{-1} luminosity is below 1 kHz. Compared with the SIDIS coincidence rate ($\sim$ 50 kHz), the requirement on DAQ for this measurement is very mild. Therefore, the current design of DAQ system for SoLID will satisfy the needs of the proposed measurement.

3.6 Background

3.6.1 Detector Resolution

Since we are interested in the exclusive electroproduction of J/Ψ, the resolution of the SoLID spectrometer is important in rejecting different backgrounds. The resolution of the SoLID spectrometer has been studied extensively by the SoLID-SIDIS collaboration [38]. Fig. 9 shows the expected momentum and angular resolution for different polar angles and momentum ranges. The position resolution of the GEM chambers is assumed to be $100\mu m$, and the angle between the u/v readout strips is assumed to be 10 degrees. Furthermore, the effects of multiple scattering due to finite thickness of the GEM chambers and the air in SoLID spectrometer are taken into account. The average momentum resolution, the average polar angular resolution, and the average azimuthal angular resolution are about 2%, 0.6 mr, and 5 mr, respectively. These expected resolutions are used to study the background rejection capability in the following sections.

3.6.2 Physics Background

Due to the large mass of J/Ψ meson and the fully exclusive kinematics of the channel of interest, we do not expect any physics background except for the Bethe-Heitler (B-H) process shown in Fig. 10. This can be seen on the left panel of Fig. 11, where we use Pythia software program to investigate if there is any physics background in our kinematics region. Here, we use reconstructed mass of J/Ψ ($M_{J/\Psi}^2$) from its electron and positron decay products and the missing mass of the entire system:

$$M_{missing}^2 = (p_e^0 + p_p^0 - p_e - p_{J/\Psi} - p_p)^2 \tag{20}$$

to ensure the exclusivity of this channel. Detector resolutions are included in these reconstructed variables. Cuts are applied to ensure exclusivity:

$$9.0 \ GeV^2 \ < \ M_{J/\Psi}^2 \ < \ 10.5 \ GeV^2 \tag{21}$$

$$-0.015 \ GeV^2 \ < \ M_{missing}^2 \ < \ 0.015 \ GeV^2. \tag{22}$$

Fig. 11 clearly shows that there is no known physics background except the B-H process in the region of interest.

The well-known two photon Bethe-Heitler process (Fig. 10) contains the same final state particles as the exclusive electroproduction of J/Ψ. The resulting electron and positron from the B-H process can have an invariant mass at 3.1 GeV, which is a background to the J/Ψ detection. In order to evaluate this background rate at our kinematics, we use the GRAPE-Dilepton [50] program, which is widely used for various studies of ep collisions. Its cross section calculation is based on exact matrix element in the electroweak theory at tree level. The expected backgrounds from the B-H process for the 3-fold (right panel) and 4-fold coincidence (left panel) are shown in Fig. 12. Compared to the expected count rate based on the 2-gluon exchange model, counting rate of the B-H
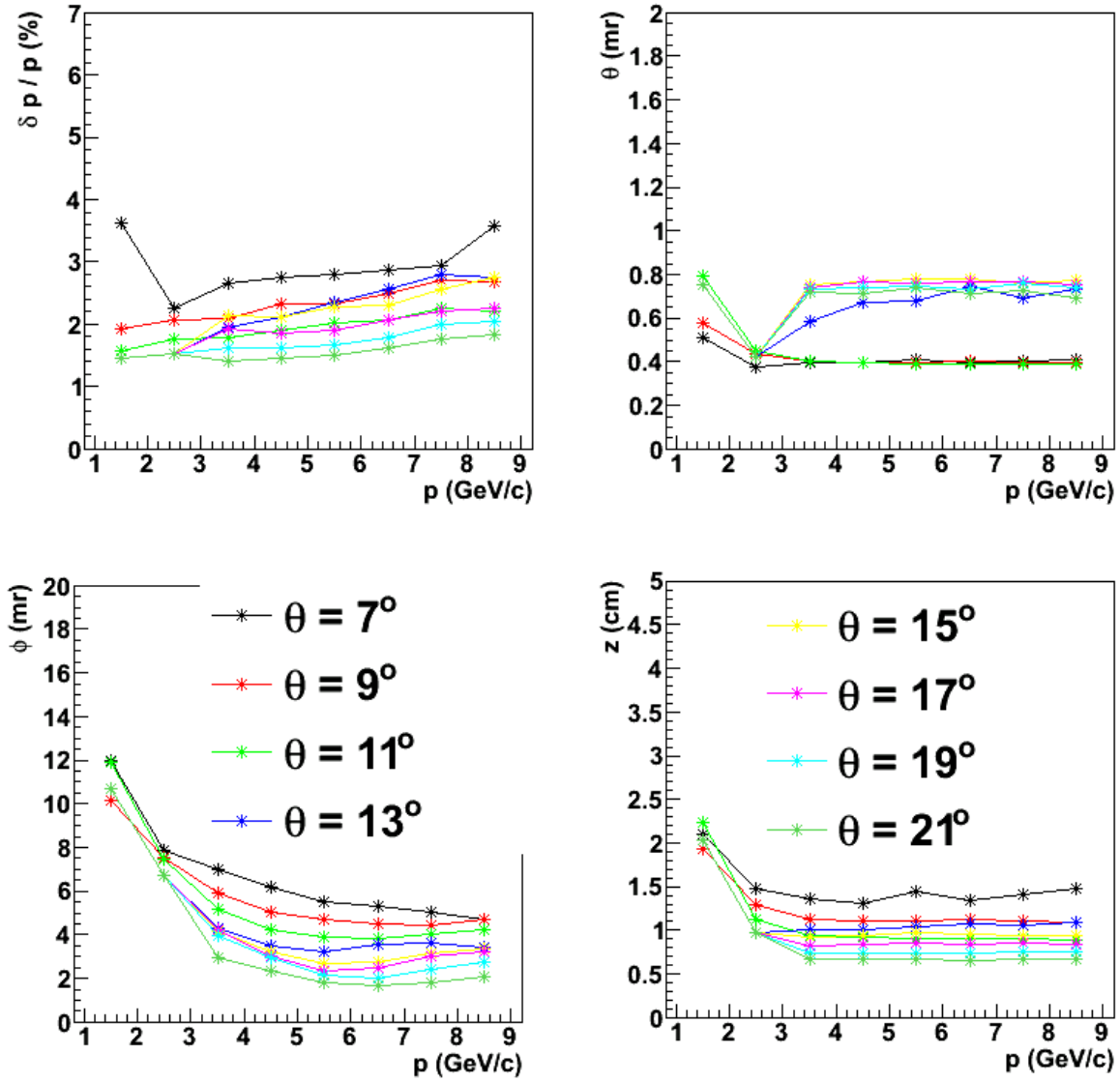
Figure 9: The expected momentum, angular and interaction vertex resolution for SoLID. The position resolution of the GEM chambers is assumed to be 100 μm. The angle between u/v readout strip is assumed to be 10 degrees.
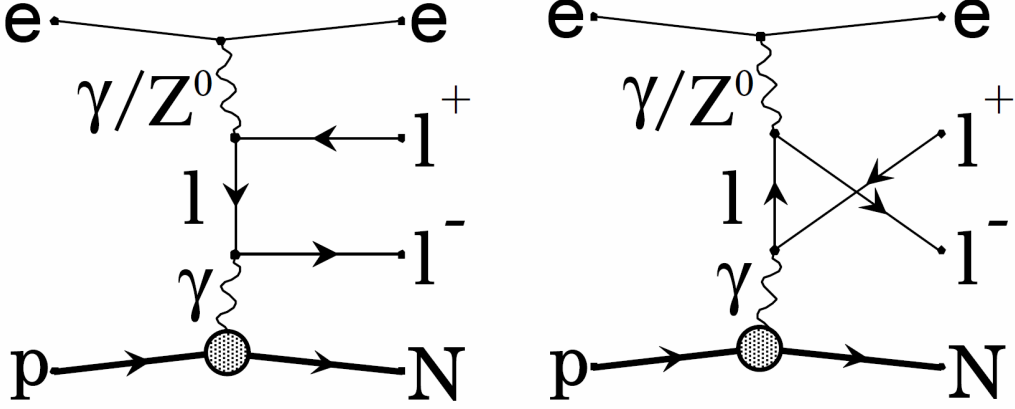
Figure 10: Two photon Bethe-Heitler process with dilepton in final state.

process is about 10%, and the contamination becomes larger when approaching the J/Ψ production threshold. The t-dependence of the B-H cross section is similar to that of J/Ψ production. Since the B-H process is well known, the background subtraction procedure would lead to negligible systematic uncertainties. The impact on statistical uncertainties is included in projections as $\frac{\sqrt{N_{signal}+N_{background}}}{N_{signal}}$, where the N_{signal} and $N_{background}$ are the expected counts from signal and background, respectively.

Furthermore, as discussed in our physics motivation, the interference term of B-H amplitude with that of J/Ψ electroproduction would reveal important information on the relative contributions of the real to the imaginary part of the $J/\Psi - N$ scattering amplitude. One would naively expect an effect of:

$$A = \frac{2 \cdot |A_{B-H} \cdot A_{J/\Psi}|}{|A_{B-H} + A_{J/\Psi}|^2} \sim \frac{2 \cdot \sqrt{|A_{B-H}|^2 \cdot |A_{J/\Psi}|^2}}{|A_{B-H}|^2 + 2 \cdot \sqrt{|A_{B-H}|^2 \cdot |A_{J/\Psi}|^2} + |A_{J/\Psi}|^2} \approx 35\% \qquad (23)$$

Such a back-of-the-envelope estimation shows that the interference term of B-H amplitude with that of J/Ψ electroproduction can be a very powerful tool to study the behavior of the $J/\Psi - N$ scattering amplitude near threshold. We are working toward developing a full theoretical prediction of such an interference.

3.6.3 Random Coincidence Background

Taking the 2-gluon model as an example, the expected rate of the electroproduction of J/Ψ near threshold is about 485 μHz. Compared with common channels measured at JLab, this is a rare channel. One background concern is the random coincidence signal. For the 4-fold coincidence, the possible combinations include:

- (e,J/Ψe)+(J/Ψp,p), (e,J/Ψp)+(J/Ψe,p), (e,p)+(J/Ψe,J/Ψp),
  (e,J/Ψe,J/Ψp)+(p), (e,J/Ψe,p)+J/Ψp, (e,J/Ψp,p)+J/Ψe, (J/Ψe,J/Ψp,p)+e
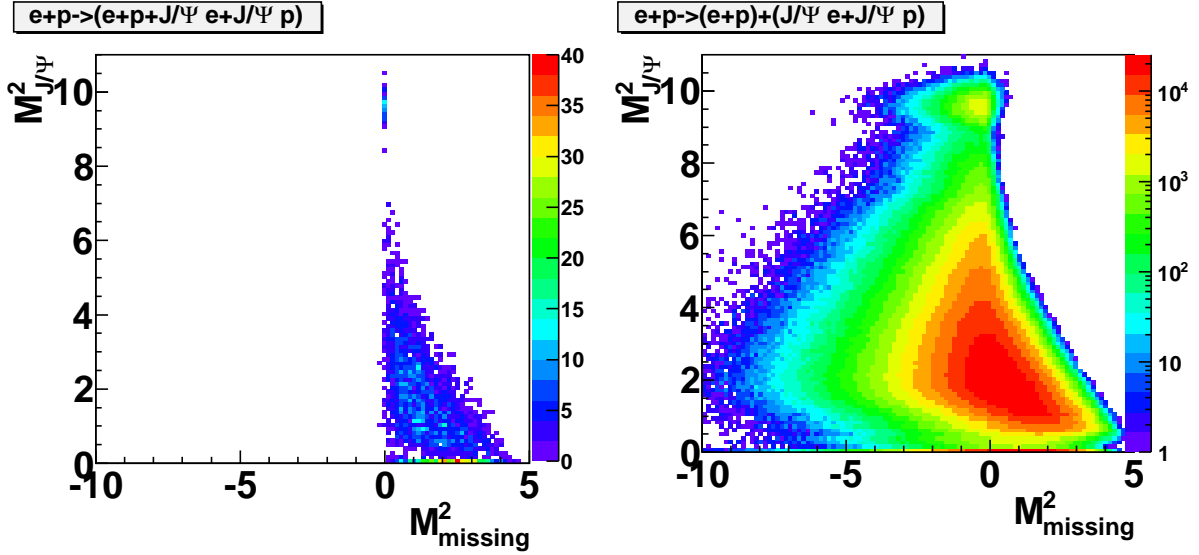
Figure 11: The reconstructed mass of the J/Ψ is plotted with respect to the missing mass of the entire system for electroproduction of J/Ψ (left panel) and for the random coincidence of an electron-proton pair with electron-positron pair from the J/Ψ decay (right panel). The expected detector resolutions of SoLID are taken into account when reconstructing these variables. The unit of both x and y axes is GeV^2.
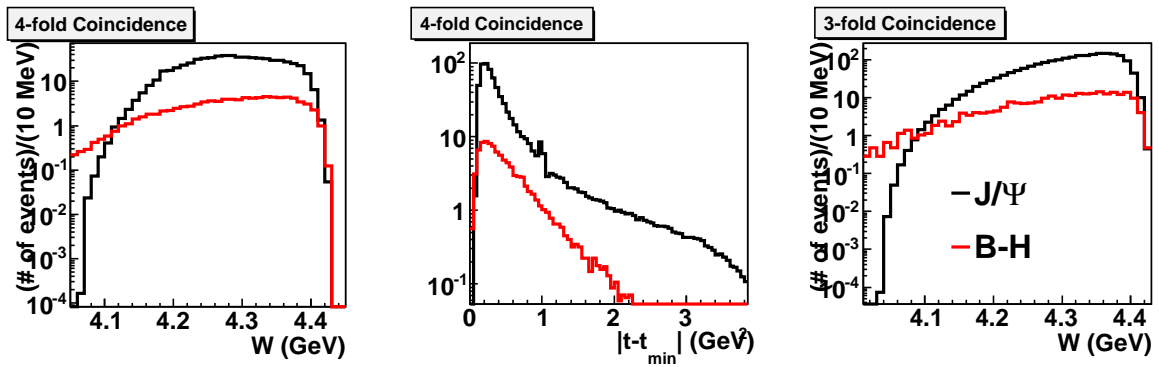
Figure 12: The expected backgrounds from B-H are shown (red lines) for the 3-fold (right) and 4-fold (left and middle) coincidence channels. The expected signals assuming a 2-gluon exchange model for J/Ψ production are shown as black lines.

- (e,J/Ψe)+J/Ψp+p, (e,J/Ψp)+J/Ψe+p, (e,p)+J/Ψe+J/Ψp, (J/Ψe,J/Ψp)+e+p, (J/Ψe,p)+e+J/Ψp, (J/Ψp,p)+e+J/Ψe

- e+J/Ψe+J/Ψp+p

Here, we use e, J/Ψe, J/Ψp, and p to represent the scattered electron, the electron and positron from the J/Ψ decay, and the recoil proton, respectively. Furthermore, particles inside parentheses "()" correspond to a real coincidence. The channels connected by "+" are part of random coincidence combinations.

In order to correctly estimate the random coincidence background, one has to estimate the rate of all the possible real coincidence channels. We used Pythia software package [51] to carry out this task. The generated kinematics range is $0.05 < y < 0.95$ and $0.1 < Q^2$. The SoLID acceptance was mimicked by the following: i) recoil proton, $P_p > 1$ GeV and $8 < \theta_p < 15$ degs, ii) scattered electron, $1 < P_e < 2.5$ GeV and $8 < \theta_e < 15$ degs, iii) electron from the J/Ψ decay, $P_{J/\Psi e} > 2.5$ GeV and $8 < \theta_{J/\Psi e} < 25$ degs, and iv) positron from the J/Ψ decay, $P_{J/\Psi p} > 2.5$ GeV and $8 < \theta_{J/\Psi p} < 25$ degs. The rate calculated from Pythia is compared with the single rate calculated by Wiser [48] and QFS [47]. Results are shown in Table. 3. While the single electron rate is consistent with the estimation of Wiser/QFS, the rate of single protons is about a factor of 4 smaller. Furthermore, Pythia over-estimates the electroproduction of J/Ψ by a factor of 100 at our kinematics.

Particle Type	Rate in Pythia	Rate by wiser/QFS/2-g
e	165 kHz	105 kHz
J/Ψe	460 kHz	413 kHz
p	306 kHz	1.3 MHz
(e+p+J/Ψe+J/Ψp)	0.015 Hz	1.57e-4 Hz

Table 3: Rate validation for Pythia.

With coincidence rates estimated from Pythia, we can calculate the random coincidence rate. For example, for (e,p)+(J/Ψe,J/Ψp) channel, the random coincidence rate can be calculated as:

$$R_{(e,p)+(J/\Psi e,J/\Psi p)} = R_{(e,p)} \cdot 6 \ ns \cdot R_{(J/\Psi e,J/\Psi p)} \cdot f_{sup}, \tag{24}$$

where the $R_{(e,p)}$ and $R_{(J/\Psi e,J/\Psi p)}$ are the true coincidence rate for (e,p) and (J/Ψe,J/Ψp), respectively. We have assumed a 6 ns coincidence window. In addition, due to the requirement of full exclusivity in kinematics, the random coincidence background will be further suppressed by f_{sup}. The right panel of Fig. 11 shows the reconstructed $M^2_{J/\Psi}$ and $M^2_{missing}$ from random pairs (e,p) and (J/Ψe,J/Ψp). Then the suppression factor f_{sup} is calculated as the ratio of number of events passing the kinematics cut to the total number of events. In the case of (e,p)+(J/Ψe,J/Ψp), the f_{sup} is calculated to be 8×10^{-5}. Table. 4 summarizes the effective random coincidence rate for different combinations. Compared

26
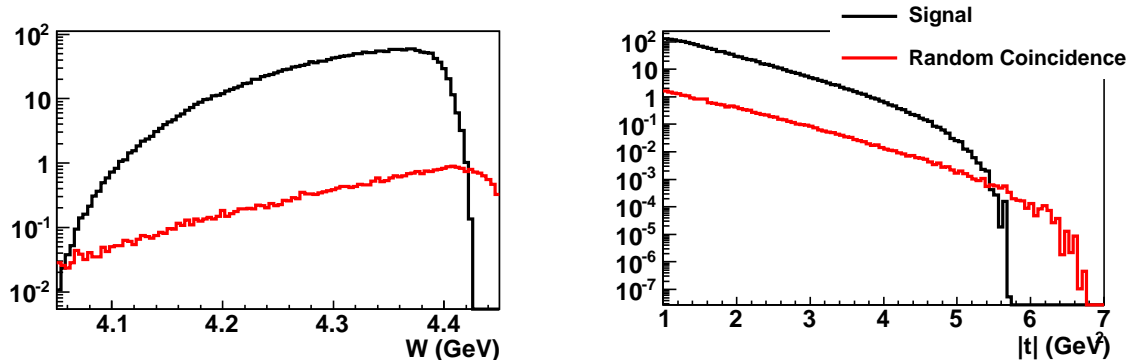
Figure 13: The random coincidence backgrounds are compared with our expected 3-fold signal based on the 2-gluon exchange model. The left (right) panel shows the comparison in W (t).

to the rate estimated of the 2-gluon exchange model, the random coincidence background is about 2.3% for the 4-fold coincidence channel and includes a factor of 3 reduction from the coincidence vertex constraint.

The study with Pythia is not totally complete. Since the Q^2 cut-off is at 0.1 GeV^2, we did not include the J/Ψ photoproduction background. On the other hand, the current J/Ψ production rate in Pythia is higher than expectation by a factor of 100. Nevertheless, from Table. 4, the dominated background is coming from a random coincidence of a real J/Ψ with a scattered electron. Therefore, we can directly estimate the random coincidence rate assuming that the dominant contribution is due to the random coincidence of a real J/Ψ and an electron. In this case, the dominant contribution of J/Ψ production is the quasi-real photoproduction at $Q^2 \sim 0$. The production cross section is modeled using the same 2-gluon exchange model. The internal radiation length is assumed to be 2%, and the external radiation length with 15 cm liquid hydrogen target is about 0.86%. The rate and spectrum of the scattered electrons that used to form the random coincidence background come from Pythia simulation, which gives a larger single electron rate than QFS. After all kinematics cuts, the remaining random coincidence background is compared with the signal spectrum in Fig. 13. The remaining contribution is below 1.5% in most of W and t range. The ratio would increase to about 10% level for $W < 4.1$ GeV, which is acceptable. In addition, a tighter cut in coincidence timing can further reduce random coincidence background. Therefore, we conclude that the random coincidence background should not be an issue at the proposed luminosity.

3.7 Projections

The expected total number of events at 10^{37}N cm^{-2} s^{-1} luminosity and 50 days of running are summarized in Table. 1. The data will be at first binned in $|t - t_{min}|$ at fixed W.
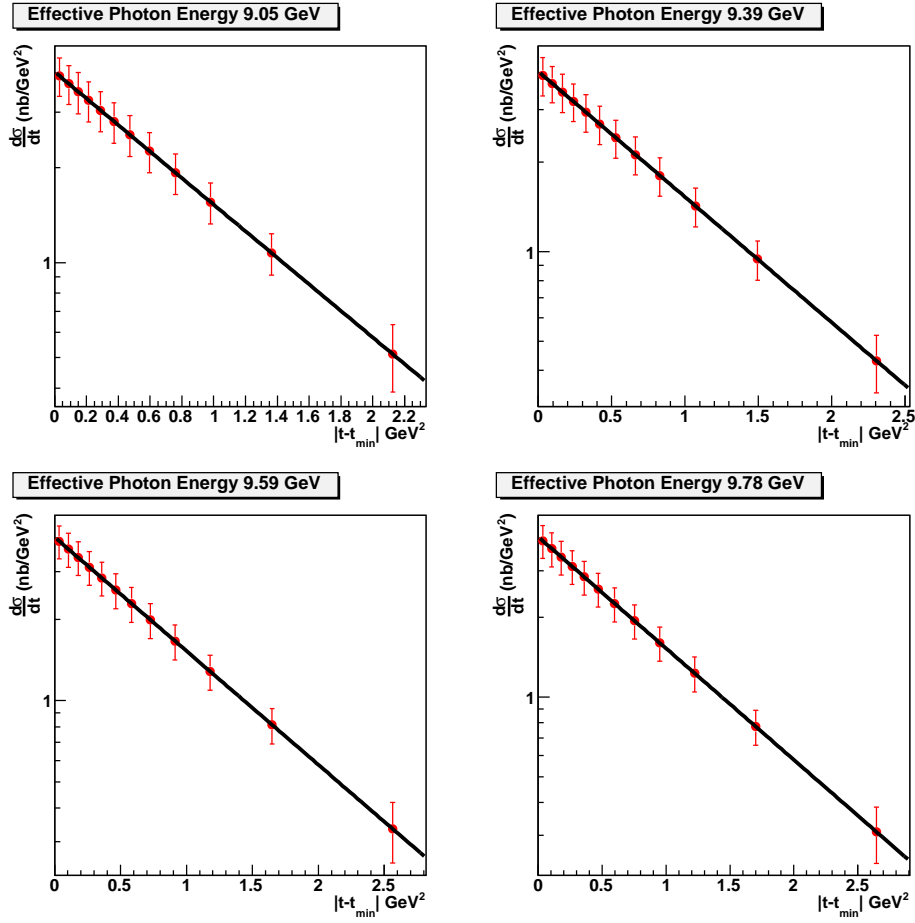
Figure 14: The example of $d\sigma/dt$ assuming the 2-gluon exchange model. The entire data set was divided into four energy bins in effective photon energy defined in Eqn. 25.

Channel I+II+III+IV	Rate of I	Rate of II	Rate of III	Rate of IV	Suppression Factor	Effective Rate (Hz)
$(e,J/\Psi e)+(J/\Psi p,p)$	0.29 kHz	0.015 kHz	N/A	N/A	3e-7	7.8e-12
$(e,J/\Psi p)+(J/\Psi e,p)$	0.035 kHz	67 kHz	N/A	N/A	5e-8	7.0e-10
$(e,p)+(J/\Psi e,J/\Psi p)$	22.3 kHz	0.04 kHz	N/A	N/A	8e-5	4.3e-7
$(e,J/\Psi e,J/\Psi p)+p$	0.01 kHz	306 kHz	N/A	N/A	9.3e-5	1.7e-6
$(e,J/\Psi e,p)+J/\Psi p$	0.04 kHz	0.13 kHz	N/A	N/A	1.3e-8	4e-13
$(e,J/\Psi p,p)+J/\Psi e$	0.0037 kHz	460 kHz	N/A	N/A	4.7e-7	4.8e-9
$(J/\Psi e,J/\Psi p,p)+e$	0.0048 kHz	165 kHz	N/A	N/A	1.75e-3	8.3e-6
$(e,J/\Psi e)+J/\Psi p+p$	0.28 kHz	0.13 kHz	306 kHz	N/A	<5e-7	1.9e-13
$(e,J/\Psi p)+J/\Psi e+p$	0.035 kHz	460 kHz	306 kHz	N/A	<5e-7	8.9e-11
$(e,p)+J/\Psi e+J/\Psi p$	22.3 kHz	460 kHz	0.13 kHz	N/A	<5e-7	2.3e-11
$(J/\Psi e,J/\Psi p)+e+p$	0.04 kHz	165 kHz	306 kHz	N/A	<5e-7	1.4e-7
$(J/\Psi e,p)+e+J/\Psi p$	67 kHz	165 kHz	0.13 kHz	N/A	<5e-7	2.5e-11
$(J/\Psi p,p)+e+J/\Psi e$	0.015 kHz	165 kHz	460 kHz	N/A	<5e-7	2e-11
$e+J/\Psi e+J/\Psi p+p$	165 kHz	460 kHz	0.13 kHz	306 kHz	<5e-7	3.1e-13
Total	N/A	N/A	N/A	N/A	N/A	1.1e-5

Table 4: Table of random coincidence rates for the 4-fold coincidence.
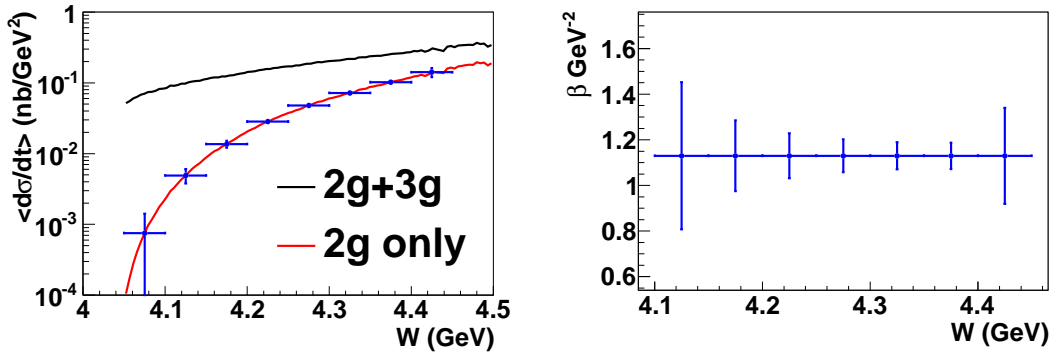
Figure 15: Left panel: Projected uncertainties for the average $< d\sigma/dt >$ (nb/GeV^2) vs. W for 50 days running at 10^{37} N cm^{-2} s^{-1} luminosity. Right Panel: Projected sensitivities for the average β (GeV^{-2}) vs. W for 50 days running at 10^{37} N cm^{-2} s^{-1} luminosity. The 2-gluon exchange only model was assumed in calculating the rates.

Fig. 14 shows examples of t-dependence assuming the 2-gluon exchange model. In this case, the entire energy range was binned into 4 bins in terms of the effective photon energy

$$E_\gamma^{eff} = \frac{W^2 - M_p^2}{2M_p}. \tag{25}$$

The projected data is then plotted against $|t - t_{min}|$ such that the average $d\sigma/dt$ as well as the slope β can be determined. The projected sensitivities for the average $d\sigma/dt$ vs. W are shown in the Fig. 15. The projections of β are shown in the right panel of Fig. 15. The uncertainty of the slope β is approximated as

$$\frac{\delta\beta}{\beta} = \sqrt{\frac{2}{N}}, \tag{26}$$

when $(t_{max} - t_{min}) \rightarrow \infty$. In making these projections, we have assumed the 2-gluon exchange only model and 3-fold coincidence channel. The resolution in W is about 0.008 GeV, which is well below the current W bin width. Our projections for the total cross sections are then plotted against the effective photon energy in Fig. 16. Together, we have also plotted the world data of J/Ψ photoproduction. The fit of 2-gluon exchange only model and (2+3)-gluon exchange model are plotted as well with dotted and solid lines, respectively. It is clear that the proposed measurements will significantly advance our knowledge of electroproduction of J/Ψ near the threshold region.

3.8 Systematic Uncertainties

The goal of this proposal is to measure the cross sections of electroproduction of J/Ψ near production threshold with SoLID . Although this would be the first experiment to measure cross sections with SoLID, the required accuracy of such a measurement is reasonable. A 15% systematic uncertainty would satisfy our needs for the search of the enhancement of cross sections near threshold region. As shown in Fig. 16, the effect between the 2-gluon only model and the (2+3)-gluon model is expected to be a factor of 2-100 depending on the effective photon energy. In the following sections, we list the major systematic uncertainties expected for such measurement.

- **Acceptance Effect:** The understanding of the acceptance would be the most challenging task for our cross section measurements with the large acceptance SoLID spectrometer. With the ability of measuring the 3-fold coincidence, we can benchmark the forward angle acceptance to a high precision. Furthermore, with the e-p elastic channel at low beam energy (2.2 and 4.4 GeV), one can validate the acceptance of forward and large angles by detecting the single electron. We expect to reach a better than 10% acceptance uncertainty for our 3-fold and 4-fold coincidence channel.
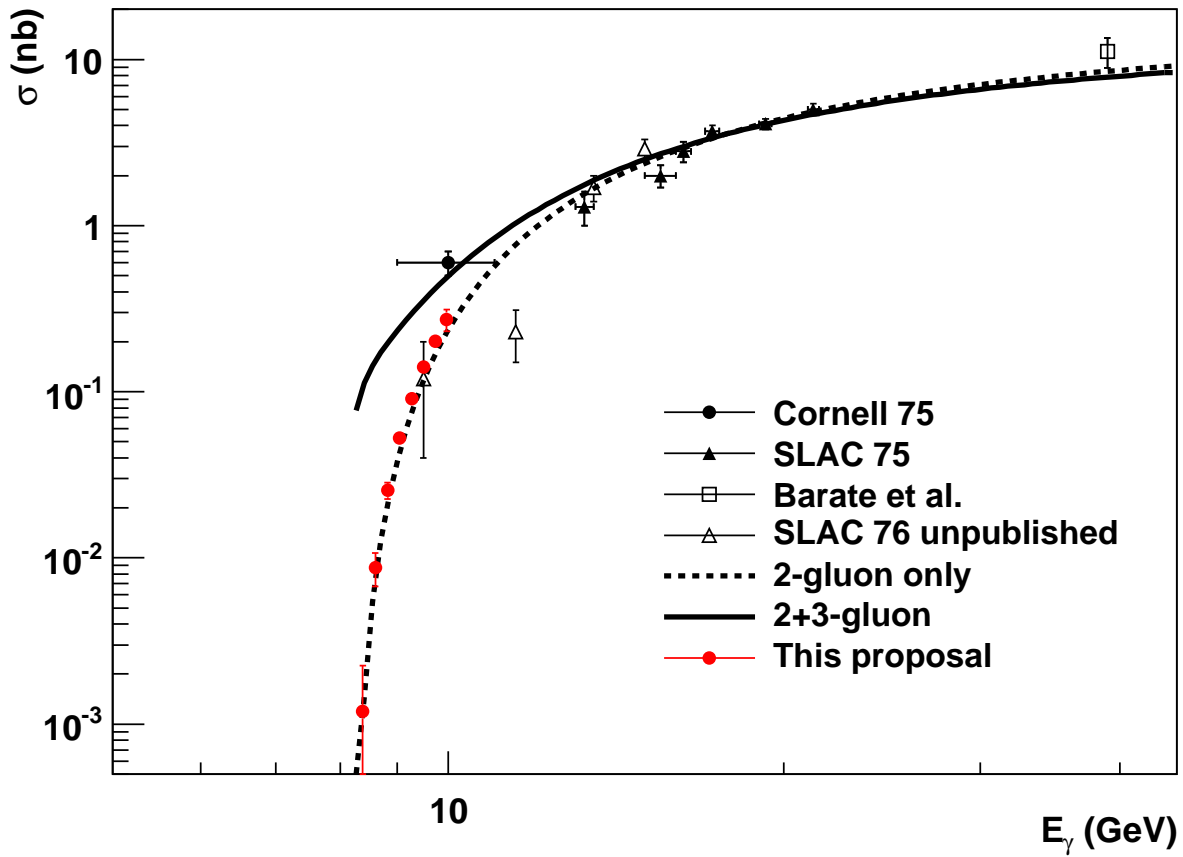
Figure 16: Projected uncertainties on total J/Ψ photoproduction cross section. Our projections are based on the 2-gluon exchange model. The central point of our projections are positioned at 1.2 times of the predicted total cross section of the 2-gluon exchange model in order to differentiate our projections from SLAC76 [23] points. The electroproduction data is plotted against effective photon energy defined in Eqn. 25.

- **Detector and Trigger Efficiency:** The current study of the tracking has indicated a high tracking efficiency. We expect a 1-2% uncertainty in the tracking efficiency. For the calorimeter, the trigger threshold (sum of energy) will be set well below the region of interest leading to a negligible trigger inefficiency. The separation of electrons from pions will preserve a >97% efficiency. We expect a 1% uncertainty in the pion rejection. For the gas Cherenkov, a detailed GEANT simulation has been carried out. The expected uncertainty is about 2%. For the efficiency of the triple coincidence trigger, a 50 ns online coincidence window has been assumed, and the resulting trigger rate is well below the designed DAQ limit. We expect to reach a 1-2% uncertainty, including dead time, individual trigger efficiency, coincidence blocking in the overall trigger efficiency.

- **Target Luminosity:**
  The standard 15 cm long liquid hydrogen target will be used for this measurement. The average beam current will be at 3 μA. At such a low beam current, the effect of target boiling will be negligible. We expect a < 2% uncertainty in the overall luminosity.

- **Contribution from Al Wall:**
  For the 15 cm long liquid hydrogen target in Hall A, the total thickness of the upstream and downstream aluminum wall is about 8 mil, corresponding to about 5% of number of nucleons compared to those in the liquid hydrogen. We will use two methods to determine the background. The first method is to apply cuts on the reconstructed vertex. The expected resolution of reconstructed vertex z position is about 1 cm for SoLID. In addition, we will also take Al dummy data for 3 days in order to study the J/Ψ electroproduction background from Al in detail. We expect to achieve a better than 1% uncertainty in Al Dummy subtraction.

- **Background Contamination:**
  The random coincidence background is expected to be at the few percent level, and is expected to be directly subtracted from the off-window events. The B-H background is expected to be at 10% level. Since the process is well known, we expect negligible systematic uncertainty in subtraction procedure. Therefore, we quote a 0.5% uncertainty due to background subtraction.

The total systematic uncertainty is thus estimated to be about 11% with a quadrature sum of all contributions listed above. Below, we list the physics processes that we will use to calibrate and check our cross section measurement.

- **Comparison to existing data of J/Ψ photoproduction:**
  Our projections in Fig. 16 show that our data will cover a wide range of effective photon energy. Part of the data would overlap with the early Cornell [21] and SLAC [23] measurements.

- **Elastic e-p scattering with 2.2 and 4.4 GeV electron beam:**
  The elastic e-p scattering is the most well understood cross section at JLab energies. We will measure the single electron, and use the missing mass technique to reconstruct the recoil proton. This channel will be used for the optics study of the SoLID magnet. We will also use it to understand the acceptance for the single particle.

- **DIS process:**
  The inclusive DIS process can be used to cross check the acceptance in addition to the aforementioned elastic e-p scattering. The approved SIDIS experiments will measure the cross section ratio of electro-pion production from hydrogen and deuteron to test the $x - z$ factorization of SIDIS [38] process. These measured cross sections can be directly compared with the precision cross section measurements from the Hall C (E12-06-104, E12-09-002 and E12-09-017). These comparisons will establish the baseline for the acceptance of SoLID and the coincidence measurements.

4 Beam Request

The beam time request is summarized in Table. 5. We request 50 days of total beam time with 3 μA, and 11 GeV electron beam on a 15 cm long liquid hydrogen target. A total overhead time of 10 days is requested. This overhead time will be shared among activities, such as detector calibration, data taking with Al dummy target, special low luminosity running for understanding the trigger efficiency and normalization for the cross section measurement. Major target/detector related down times can also be arranged to coincide with the scheduled accelerator maintenance activities in order to reduce overhead time.

	Time (Hour)	Time (Day)
Production on LH2 at 11 GeV	**1200**	50
Dedicated Al Dummy Run	72	3
Optics and detector check	72	3
Special low luminosity running	96	4
Total Time Request	**1440**	**60 days**

Table 5: Summary of the beam time request.

5 Summary

We propose to measure the cross section of the full exclusive electroproduction of J/Ψ near threshold (4.05 GeV $<$ W $<$ 4.45 GeV and $|t - t_{min}| < 2.5$ GeV^2) to study QCD in the non-perturbative regime. For this experiment, we will utlize the SoLID spectrometer, the 11 GeV electron beam and a 15 cm long liquid hydrogen target at a luminosity of 10^{37} N cm^{-2} s^{-1}. We request 60 days beam time in total.

6   Appendix: Experimental Setup and Particle Identification

6.1   SoLID Magnet and Acceptance

Our design is based on the CLEO-II magnet. It is a solenoidal magnet with a uniform axial central field of 1.5 T, a large inner space with a clear bore diameter of 2.9 m and a coil of 3.1 m diameter. With a coil length of 3.5 m and a cryostat of 3.8 m, its field uniformity is $\pm 0.2\%$. The coil is 5×16 mm^2 aluminum stabilized superconductor and run at 3300 A to balance the heat generated in the leads as well as the large conductor size with its simpler construction and ease of protection. The current return yoke has 3 layers with 36 cm thickness each and is octagonally divided. The setup arrangement is exhibited in Fig. 17

Taking the CLEO magnet condition into account and considering the requirements of the SoLID approved experiments (PVDIS and SIDIS), the SoLID collaboration has produced two yoke design versions for the CLEO magnet to accommodate both experimental setups. The SIDIS version of the yoke fits well in this proposed experiment with a minimum modification [10]. The 2D magnetic field map is evaluated using the program Poisson Superfish [53].

The acceptance of SoLID for the electroproduction of J/Ψ has been studied using a GEANT program. Fig. 18 shows the momentum vs. polar angle for all four particles that fall into the SoLID acceptance. The scattered electron and the recoil proton are only detected by the forward angle detector. The electron-positron pair from the J/Ψ decay is captured mainly by the large angle detector. Some very high momentum ($P > 5$ GeV) electron/positron from J/Ψ decay will be identified by the forward angle detector as well. The gap shown in the top right panel of Fig. 18 for the electron from the J/Ψ decay reflects the fact that the large angle and forward angle detector packages are physically separated. Kinematics of the reaction dictate that each of the leptons of the J/Ψ decay pair (e^-/e^+) will carry a momentum greater than 3 GeV that coincides nicely with the specifications of the large angle calorimeter. Furthermore, the SoLID hadron detection capability enables the 4-fold coincidence detection. This in turn provides a better signal to background ratio than the 3-fold coincidence channel and a cross check to the 3-fold coincidence result.

6.2   GEM Tracker and Tracking

A total of six layers of GEM tracking detectors will be used to provide the momentum, angle and interaction vertex of the particles detected. They will be placed uniformly inside the magnet. For the forward angle detectors, five layers (except for the first layer) of GEM

---

[10] The proposed measurement would require a slightly larger opening angle to detect the J/Ψ electron/positron decay pair. This can be achieved by adding an iron barrel to effectively move the front end cap upstream.
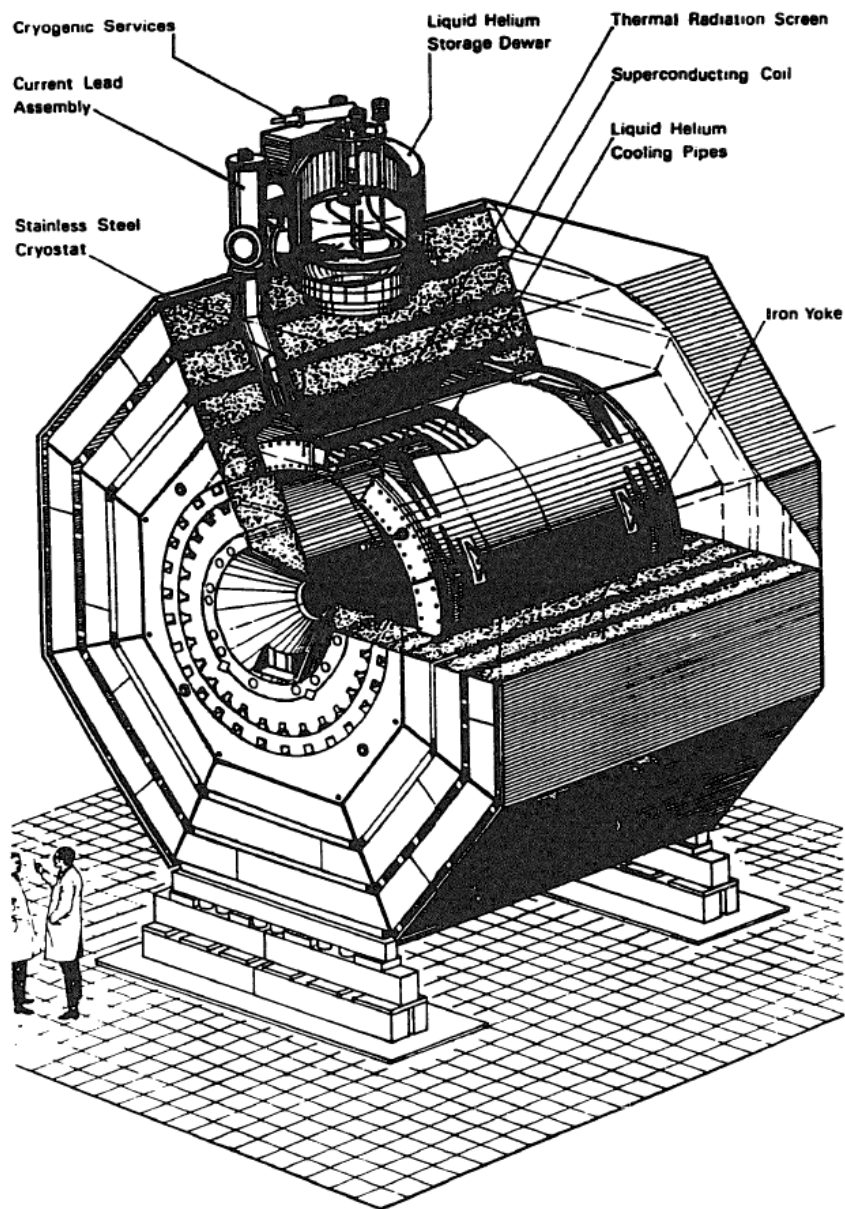
Figure 17: Arrangement of the CLEO II superconducting coil and steel magnet yoke, taken from [52].
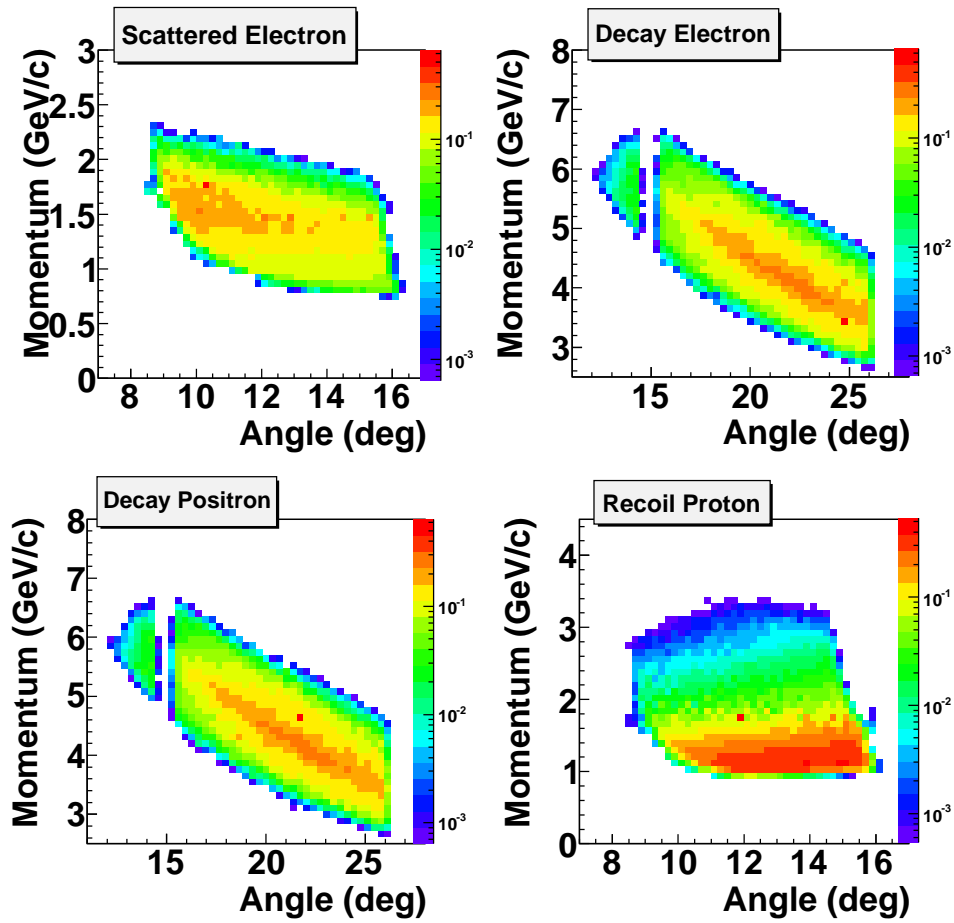
Figure 18: The simulated momentum vs. polar angle for all produced particles from J/Ψ electroproduction.

detectors will be used. In principle, three points are needed to reconstruct the kinematic variables. The fourth and fifth points will bring enough redundancy to compensate for the inefficiency of the GEM tracking detector. For the large angle detector, the first four layers of GEMs detector will provide the momentum, angle and vertex reconstruction. In this case, four layers of GEMs detector are enough since the background level in the large angle kinematics is expected to be smaller.

Each of the GEM layers will cover 360 degrees. The GEM detectors are used with 2-D readouts. The induction electrode contains two sets of stripes or pads, insulated from each other. The angle between the two readout directions depends on the width of one sector, which may be selected in a range of $9° - 12°$ depending on the plane. The amplitude correlation of the signals from the two planes allows for a suppression of the false U-V combination by a factor of $\sim$ 3-5 in reducing fake hits. The background rates from the GEM detectors have been investigated using GEANT with all physics processes turned on (Moller/Mott ... etc). Studies in Hall A show that the wire chamber background rates can be predicted by GEANT within a 50% level with 6 GeV electron beam [49]. Results of the background estimation of the current SoLID setup are shown in Fig. 19. The GEMs have been used in a 30 kHz/mm^2 flux in the COMPASS experiment, which is much higher than the estimated rates in our configuration. The tracking efficiency has been studied extensively in the SIDIS experimental configuration [38] of SoLID, which is similar to our configuration. Therefore, we do not expect any issue in achieving a high tracking efficiency in this experiment.

6.3   Electromagnetic Calorimeter

Electromagnetic calorimeters (EC) based on the Shashlyk design [54] will be used for electron detection in both the forward and large angle detectors. They will provide the basic trigger. A Shashlyk calorimeter is a sampling calorimeter constructed from alternating layers of scintillator and heavy absorber such as lead. Scintillation light is absorbed, re-emitted and transported to the photon detector by wave-length shifting (WLS) optical fibers penetrating through the calorimeter modules longitudinally along the impact particle direction. The background rates of the calorimeters are shown in Fig. 21. The overall energy flux is about a factor of 2 higher than that of the SIDIS experiment [38] configuration.

The current Shashlyk calorimeter module design is based on the COMPASS module as shown in Fig. 20. A GEANT simulation was used to study the key specifications for optimal physics results and lower cost. Our module will consist of 183 layers (about 21 radiation lengths). Each layer consists of a 1.5 mm thick scintillator plate and a 0.6 mm lead plate thickness. This is to provide a fine sampling, and therefore an energy resolution of $5\%/\sqrt{E}$ is achieved with an effective radiation length about 21 mm. A preshower and a shower part in the EC is essential to reach the required pion rejection 100:1 with 97% electron efficiency. The preshower thickness of 3-5 radiation lengths can maximize the difference in energy deposition between electrons and pions. The design of a unified
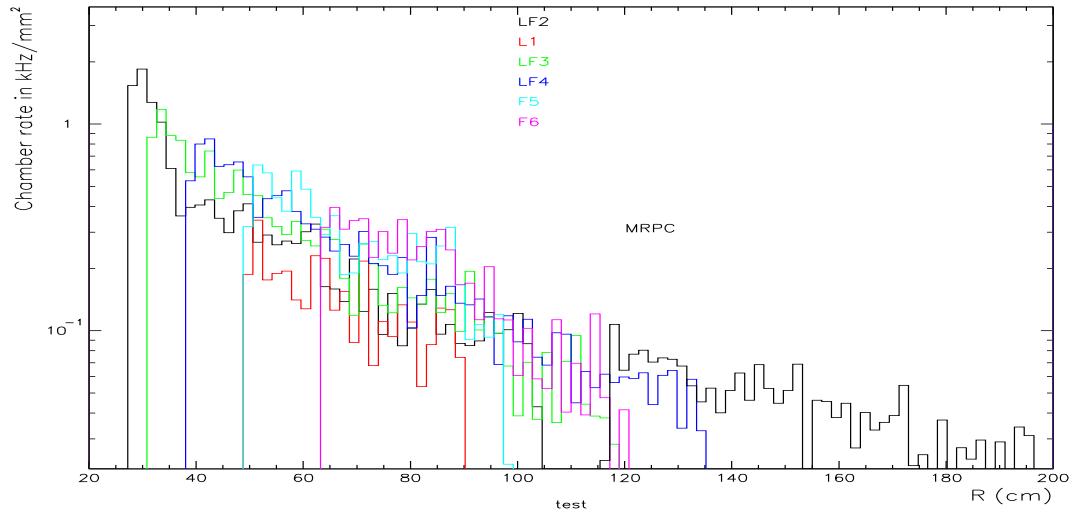
Figure 19: The results of simulated background for 11 GeV beam are presented. The x-axis labels the GEM radius and the y-axis represents the rate. There are six layers of GEM detectors in total. The "L1" labels the first layer in the large angle. "LF2", "LF3" and "LF4" are shared between the large angle and forward angle detection. The "F5" and "F6" are used in the forward angle only.
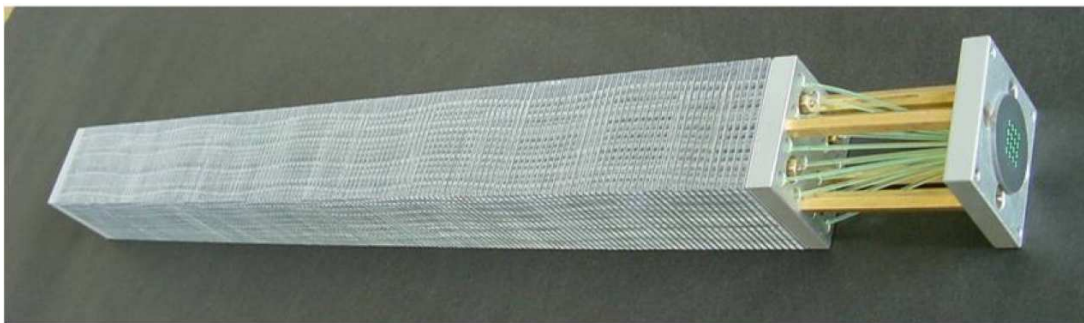
Figure 20: A Shashlyk calorimeter module produced by the institute for High Energy Physics of Russia for the COMPASS experiment.
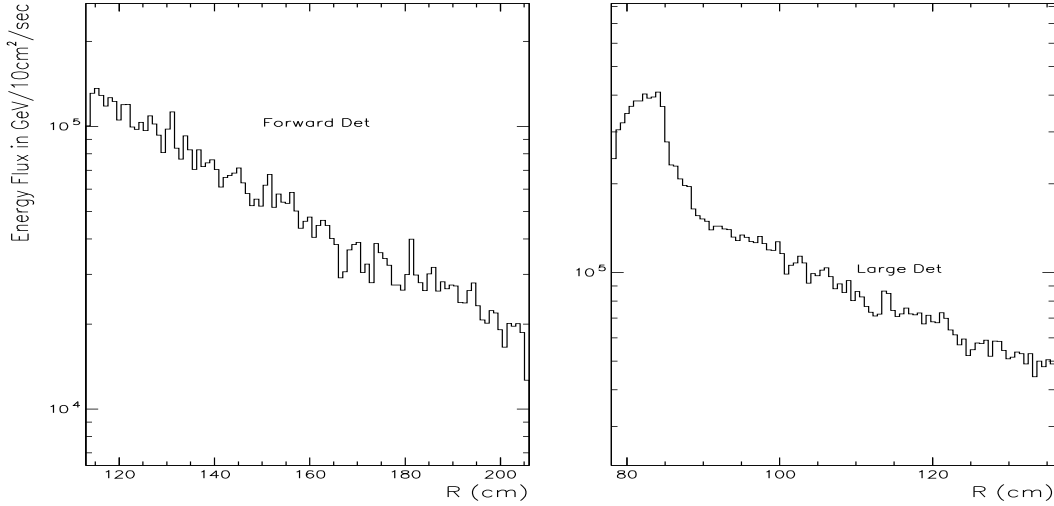
Figure 21: The left panel shows the background in the calorimeter for the forward angle detector and the right panel shows the background in the calorimeter for the large angle detector at 11 GeV. The x-axis is the radius of the calorimeter and the y-axis is the energy flux.

preshower and shower module is being considered in which the preshower and shower segments are readout by different fibers. The preshower fibers need to be optically isolated from the shower part. The lateral size of each module determines the position resolution and the background level of the reconstructed shower hits. The lateral size of about 10 cm will provide a good balance between position resolution and cost.Furthermore, the scintillators and fibers will have a time response about a few hundred picoseconds, which has been achieved in the COMPASS module design. Such a timing resolution will satisfy the needs of coincidence trigger formation. At the chosen luminosity of 10^{37} N cm^{-2} s^{-1} for this experiment, the radiation level at the EC is expected to reach 100 krad per PAC month. The COMPASS module has been tested up to 500 krad. By increasing the thickness of the first few lead layers and using more radiation resistant scintillator and fibers, the radiation hardness can be further improved.

6.4 Gas Cherenkov Detector

In the proposed measurement, the identification of the scattered electrons will be provided by a threshold gas Cherenkov counter. This detector will be filled with CO_2 at 1 atm leading to a detection of electrons above 21 MeV momentum and a rejection of pions up to 4.65 GeV momentum. The gas volume extends 2.1 m along the beam line inside the magnet. The photon detectors will be positioned after the SoLID coil. The close proximity

to the SoLID magnet requires careful consideration of various options of photon detectors. The detector optical system will provide full coverage in the azimuthal angle.

A GEANT simulation was used to optimize the design of the optical system and to describe the photon detector response. It was found that with just one system of 30 spherical mirrors (following the SoLID sectoring) near perfect collection efficiency > 95%, can be achieved with a $6'' \times 6''$ active photon detector area using Winston cones. A schematic of this setup is shown in Fig. 22 where Cherenkov photons (green) produced by the passage of electrons (red) through the radiator gas are reflected by a spherical mirror (grey) in each of the 30 sectors and focused onto the photon detectors (cyan). This design consists of one-mirror optical system per sector.

Two options are under consideration for the photon detectors. One is the "PMTs" option where magnetic field resistant photomultiplier tubes, PMTs, (Fig. 22, left panel) in combination with Winston cones are used. The other is the "GEMs + CsI" option where gaseous electron multipliers with a photocathode of Cesium Iodine coating (Fig. 22, right panel) are used for the photon detector.

In the PMTs option, the Hamamatsu model H8500C-03- PMT is considered. It is a 2" multi-anode PMT with up to 94% photocathode coverage and good quantum efficiency down to wavelengths of 200 nm. These characteristics make this model ideal for tiling and we plan to use 9 such PMTs per sector, in a 3×3 array, to cover a $6'' \times 6''$ area. Early investigations of field effects (mainly in the longitudinal direction) at Temple University and further extensive studies at Jefferson Lab lead us to conclude that this device is fairly resistant in magnetic field: such unshielded PMT experiences up to 40% gain reduction in 100 Gauss field transverse to the face of the PMT which can be easily shielded. However, this loss is only about 25% in the longitudinal direction (normal to the face of the photomultiplier) and tend to decrease to 20% as the field increases to values as large as 400 Gauss. Additional tests at Jefferson Lab to ensure suitability in high-background environment are being conducted during the g2p experiment in Hall A.

An estimate of the number of photoelectrons for this option with the configuration described above (Fig. 22, left panel) yields between 25 and 35 photoelectrons. The number depends slightly on the electron polar angle: because of the mirror positioning in the tank, electrons with larger polar angles traverse a longer path in the radiator gas than those with smaller polar angles. This estimate includes wavelength dependent corrections like mirror and Winston cones reflectivities and the PMTs quantum efficiency as well as an overall correction of 0.8 to account for the reduction in the photocathode effective area as a result of tiling.

As an alternative to PMTs, the GEM + CsI option has the advantage of being very resistant to the magnetic field. This has been used successfully as a photon detector during PHENIX experiment at BNL in a Hadron Blind Detector [55]. Studies using a prototype detector by a Stony Brook group at Jefferson Lab during the g2p experiment are underway and the results will be known perhaps by the time of the PAC. The photon detector consists of three layers of GEMs, the first being covered with CsI which acts as a photocathode. The operational regime for CsI is the ultraviolet (UV) region, between
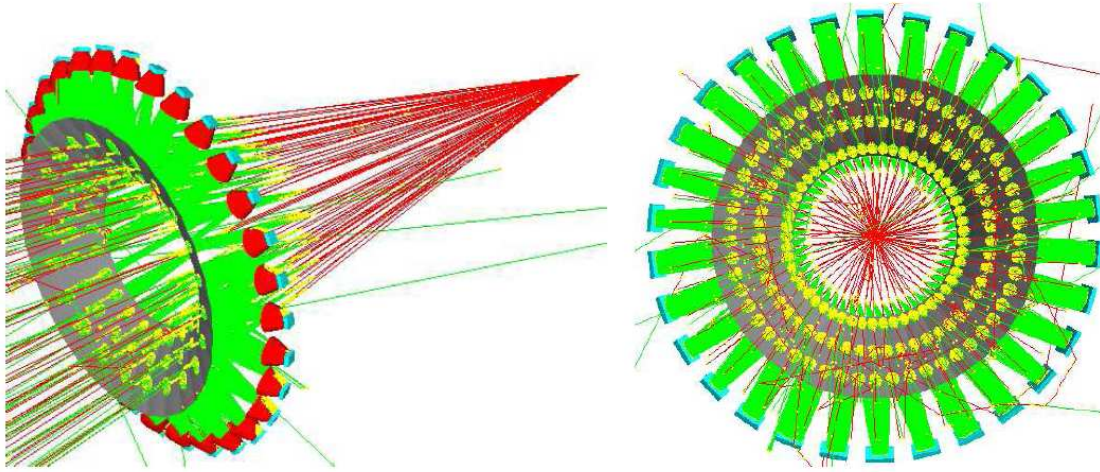
Figure 22: Setup of the light-gas Cherenkov: a system of 30 spherical mirrors (grey) will focus the Cherenkov photons (green) created by the passage of electrons (red) through a radiator gas onto photon detectors (cyan). Left panel: setup for the PMT option, side view. Right panel: setup for the GEM+CsI option, back view - as seen from the beam dump.

120 and 200 nm [56]. This requires a radiator gas with good transparency in the UV and with very good purity to avoid photon absorption by impurities. A suitable gas for the GEM + CsI option is CF_4 which, unlike CO_2, is transmissive between 120 nm and 200 nm [57]. This gas would still give an acceptable threshold for electron-pion separation and it was the gas of choice for the successful PHENIX run.

The number of photoelectrons for this option was estimated using the GEANT simulation and assuming a 12" × 12" photon detector (Fig. 22, right panel). A signal of 20 to 30 photoelectrons was obtained. Wavelength dependent corrections as mirror reflectivity and quantum efficiency of CsI were taken into account as well as an overall correction of 0.54 to account for loss of signal due to gas transparency, reduced photocathode coverage of the GEM (about 20% of the GEM surface is occupied by holes), transport efficiency of avalanche electrons through gas, etc.... This is particularly important for the GEM + CsI option where it is technically challenging to manufacture and maintain mirrors with good reflectivity in the deep UV region.

6.5 Time of Flight Detector

A layer of multi-resistive plate chamber (MRPC) detector will be inserted before the forward angle calorimeter. MRPC has been recently used in RHIC STAR and LHC ALICE as their TOFs and its typical time resolution is better than 80 picosecond. Furthermore, as a gas chamber, the MRPC does not need PMTs for readout and thus it can operate
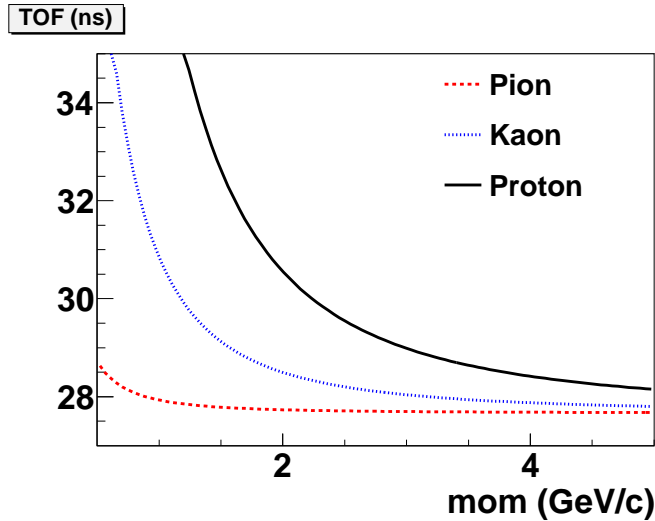
Figure 23: Particle identification through Time-Of-Flight for proton/pion/kaon.

inside a magnetic field. The simulated background rates on the MRPC (Fig. 19) are shown to be less than 0.1 kHz/mm². Studies [58] show that the MRPC can work in a environment of background rates of 0.28 kHz/mm².

The total path length from the target is about 8.3 meters. The flight time of particles is calculated by comparing the TOF signal and the beam RF signal. The differences of the TOF of different particles are plotted in Fig. 23. At 3 GeV momentum, which is about the maximum momentum of proton for this channel, the separations between proton/kaon and proton/pion are about 0.95 ns and 1.3 ns, respectively. For the TOF detector, we expect to achieve a 100 picosecond resolution. Therefore, the proton identification can be achieved for the entire momentum. For this measurement, we do not require the heavy gas Cherenkov detector. However, with the ability of the heavy gas Cherenkov, we can further reject high momentum pions, since they will start triggering the heavy gas Cherenkov starting at 2.2 GeV.

6.6   Target

We plan to use the standard Hall A 15 cm LH$_2$ target. The cell is a horizontal Al cylinder in a cigar shape. The upstream windows is separated from the rest of the cell and it can be made with thickness of 102 μm (4 mil). The wall and the downstream window are in one piece. The wall thickness is about 178 μm and the downstream window can be made 102 μm (4 mil) thick. Its diameter is about 3.81 cm. The cell can take over 100 μA electron beam, withhold over 100 psi pressure. All features of the cell can easily satisfy what is needed for this experiment, namely 3 μA current and < 2% uncertainty of the overall luminosity. The only change we need to make is to remove the flow diverter

so that the acceptance can reach 26 degrees opening angle required for the experiment. Because the experiment runs at very low current of 3 μA, the boiling effect is negligible and thus the flow diverter can be removed.

References

[1] S. J. Brodsky and G. A. Miller. Is J/Ψ - nucleon scattering dominated by the gluonic van der Waals interaction? *Phys. Lett.*, **B412**:125–130, 1997.

[2] S. J. Brodsky, I. A. Schmidt, and G. F. de Teramond. Nuclear bound quarkonium. *Phys. Rev. Lett.*, **64**:1011, 1990.

[3] M. E. Luke, A. V. Manohar, and M. J. Savage. A QCD Calculation of the interaction of quarkonium with nuclei. *Phys. Lett.*, **B288**:355–359, 1992.

[4] A. B. Kaidalov and P. E. Volkovitsky. Heavy quarkonia interactions with nucleons and nuclei. *Phys. Rev. Lett.*, **69**:3155–3156, 1992.

[5] G. F. de Teramond, R. Espinoza, and M. Ortega-Rodriguez. Proton proton spin correlations at charm threshold and quarkonium bound to nuclei. *Phys. Rev.*, **D58**:034012, 1998.

[6] V. I. Shevchenko. Nonperturbative effects in the nonrelativistic hadron scattering. *Phys. Lett.*, **B392**:457–462, 1997.

[7] A. Hayashigaki. J/Ψ nucleon scattering length and in-medium mass shift of J/Ψ in QCD sum rule analysis. *Prog. Theor. Phys.*, **101**:923–935, 1999.

[8] K. Yokokawa, S. Sasaki, T. Hatsuda, and A. Hayashigaki. First lattice study of low-energy charmonium-hadron interaction. *Phys. Rev.*, **D74**:034504, 2006.

[9] T. Kawanai and S. Sasaki. Charmonium-nucleon potential from lattice QCD. *Phys. Rev.*, **D82**:091501, 2010.

[10] K. Tsushima, D. H. Lu, G. Krein, and A. W. Thomas. J/Ψ-nuclear bound states. *Phys.Rev.*, **C83**:065208, 2011.

[11] K. Tsushima, D. H. Lu, G. Krein, and A. W. Thomas. J/Ψ mass shift and J/Ψ-nuclear bound state. *AIP Conf. Proc.*, **1354**:39–44, 2011.

[12] M. Binkeley et al. J/Ψ Photoproduction from 60 to 300 GeV/c. *Phys. Rev. Lett.*, **48**:73, 1982.

[13] B. H. Denby et al. Inelastic and Elastic Photoproduction of J/Ψ (3097). *Phys. Rev. Lett.*, **52**:795, 1984.

[14] M. D. Sokoloff et al. An Experimental Study of the a-Dependence of J/Ψ Photoproduction. *Phys. Rev. Lett.*, **57**:3003, 1986.

[15] R. Barate et al. Measurement of J/Ψ and Ψ' real photoproduction on ^{6}Li at a mean energy of 90 GeV . *Z. Phys.*, **C33**:505, 1987.

[16] P. L. Frabetti et al. A Measurement of elastic J/Ψ photoproduction cross-section at fermilab E687. *Phys. Lett.*, **B316**:197, 1993.

[17] S. Aid et al. Elastic and inelastic photoproduction of J/Ψ mesons at HERA. *Nucl. Phys.*, **B472**:3, 1996.

[18] J. Breitweg et al. Measurement of inelastic J/Ψ photoproduction at HERA. *Z. Phys.*, **C76**:599, 1997.

[19] S. Aid et al. Photoproduction of of J/Ψ Mesons in ep Collisions at HERA. *Nucl. Phys.*, **B472**:2, 1996.

[20] U. Camerini et al. Photoproduction of the Ψ Particles. *Phys. Rev. Lett.*, **35**:483, 1975.

[21] B. Gittelman et al. Photoproduction of the Ψ (3100) Meson at 11-GeV. *Phys. Rev. Lett.*, **35**:1616, 1975.

[22] B. Knapp et al. Photoproduction of Narrow Resonances. *Phys. Rev. Lett.*, **34**:1040, 1975.

[23] R. L. Anderson. Excess Muons and New Results in Ψ Photoproduction. SLAC-PUB-1471.

[24] D. Kharzeev. Quarkonium interactions in QCD. 1995. nucl-th/9601029.

[25] D. Kharzeev, H. Satz, A. Syamtomov, and G. Zinovjev. J/Ψ photoproduction and the gluon structure of the nucleon. *Eur. Phys. J.*, **C9**:459–462, 1999. 8 pages, latex, 4 figures Report-no: BI-TP 98/36.

[26] S. J. Brodsky, E. Chudakov, P. Hoyer, and J.M. Laget. Photoproduction of charm near threshold. *Phys. Lett.*, **B498**:23–28, 2001.

[27] A. Sibirtsev, S. Krewald, and A. W. Thomas. Systematic analysis of charmonium photoproduction. *J. Phys.*, **G30**:1427–1444, 2004.

[28] M. A. Shifman, A. I. Vainshtein, and V. I. Zakharov. Photoproduction of Charmed Particles and Asymptotically Free Field Theories. *Phys. Lett.*, **B65**:255, 1976.

[29] V. A. Novikov, M. A. Shifman, A. I. Vainshtein, and V. I. Zakharov. Charm Photoproduction and Quantum Chromodynamics. *Nucl. Phys.*, **B136**:125, 1978.

[30] . A. Shifman, A. I. Vainshtein, and V. I. Zakharov. Remarks on Charm Electroproduction in QCD. *Nucl. Phys.*, **B136**:157, 1978.

[31] A. Sibirtsev and M. B. Voloshin. The Interaction of slow J/Ψ and Ψ' with nucleons. *Phys. Rev.*, **D71**:076005, 2005.

[32] Rinaldo Baldini Baldini, Simone Pacetti, and Adriano Zallo. Point-like Baryons? 2008.

[33] M. Ablikim et al. Spin-Parity Analysis of $p\bar{p}$ Mass Threshold Structure in J/ψ and ψ' Radiative Decays. *Phys.Rev.Lett.*, 108:112003, 2012. 5 pages, 3 figures, submitted to Phys. Rev. Lett.

[34] J. J. Wu, R. Molina, E. Oset, and B. S. Zou. Prediction of narrow n^* and λ^* resonances with hiddne charm above 4 gev. *Phys. Rev. Lett.*, **105**:232001, 2010.

[35] P. Bosted, J. Dunne, C. A. Lee, P. Junnarkar, M. Strikman, et al. Search for Sub-threshold Photoproduction of J/Ψ Mesons. *Phys. Rev.*, **C79**:015209, 2009.

[36] Contact Person: E. Chudakov, PAC32 PR12-07-106 The A-dependence of J/Ψ Photoproduction near Threshold.

[37] Contact Person: P. Souder, PAC34 http://hallaweb.jlab.org/collab/PAC/PAC34/PR-09-012-pvdis.pdf.

[38] Contact Person: H. Gao, PAC34 http://hallaweb.jlab.org/collab/PAC/PAC34/PR-09-014-transversity.pdf.

[39] Contact Person: J. Huang, PAC37 http://www.jlab.org/exp_prog/PACpage/PAC37 /proposals/Proposals/New Proposals/PR-11-007.pdf.

[40] Contact Person: H. Gao, PAC38 http://wwwold.jlab.org/exp_prog/proposals/11/PR12-11-108.pdf.

[41] X. Qian et al. Study of the $A(e, e'\pi^+)$ Reaction on ^{1}H, ^{2}H, ^{12}C, ^{27}Al, ^{63}Cu and ^{197}Au. *Phys. Rev.*, **C81**:055209, 2010.

[42] S. J. Brodsky et al. Photoproduction of charm near threshold. *Phys. Lett.*, **B498**:23, 2001.

[43] K. Schilling and G. Wolf. How to analyze vector meson production in inelastic lepton scattering. *Nucl. Phys.*, **B61**:381, 1973.

[44] R. Fiore et al. Exclusive J/Ψ electroproduction in a dual model. *Phys. Rev.*, **D80**:116001, 2009.

[45] C. Adloff et al. Elastic Electroproduction of ρ Mesons at HERA. *Eur. Phys. J.*, **C13**:371, 2000.

[46] L. W. Whitlow. Ph. D. thesis, Stanford University, SLAC-Report-357 (1990).

[47] Developed by J. W. Lightbody and J. S. O'Connell in 1988.

[48] D. E. Wiser. Ph. D. thesis, Univ. of Wisconsin (1977).

[49] X. Qian. *Measurement of Single Target-Spin Asymmetry in Semi-Inslusive $n^\uparrow(e, e'\pi^\pm)$ Reaction on a Transversely Polarized ^3He Target*. PhD thesis.

[50] T. Abe. GRAPE dilepton (Version1.1): A Generator for dilepton production in ep collisions. *Computer Physics Communications*, **136**:126, 2001.

[51] PYTHIA. *http://projects.hepforge.org/pythia6/*, 2006.

[52] Y. Kubota et al. Superfish-a Computer Program for Evaluation of RF Cavities with Cylindrical Symmetry. *Nucl. Instr. and Meth.*, **A320**, 1992.

[53] Poisson Superfish, http://laacg1.lanl.gov/laacg/services/download_sfp.html.

[54] G. Atoian et al. An improved Shashlyk Calorimeter. *Nucl. Instr. and Meth.*, **A584**(3):291, 2008.

[55] W. Anderson et al. Design, Construction, Operation and Performance of a Hadron Blind Detector for the PHENIX Experiment. arXiv:1103.4277 [physics.ins-det].

[56] B. Azmoun et al. Collection of Photoelectrons and Operating Parameters of CsI Photocathode GEM Detectors. *IEEE Trans. Nucl. Sci.*, **56-3**:1544, 2009.

[57] C. Lu and K. T. McDonald. Properties of reflective and semitransparent CsI photocathodes. *Nucl. Instr. and Meth.*, **A343**:135, 1994.

[58] Y. Wang et al. A prototype of a high rating MRPC. *Chinese Phys.*, **C33**:374, 2009.